ICARUS 113, 331–352 (1995)

Accretion in the Roche Zone: Coexistence of Rings and Ringmoons

ROBIN M. CANUP AND LARRY W. ESPOSITO

Laboratory for Atmospheric and Space Physics, University of Colorado, Box 392, Boulder, Colorado 80309-0392
E-mail: canup@sargon.colorado.edu

Received February 15, 1994; revised July 21, 1994

Traditional accretion simulations predict rapid accumulation of ring debris into single satellites, while most theories of ring formation dismiss any accretion within the classical Roche limit. The former contradicts the continued presence of planetary rings, while the latter fails to adequately account for the many small satellites observed within ring systems. The coexistence of rings and small satellites thus challenges the premise of a strict boundary between accreting and nonaccreting regions. We have developed an accretion model designed to better examine accumulation processes in the dynamically transitional regime of outer planetary rings. We utilize "three-body" capture criteria, motivated by the work of Ohtsuki (1993 *Icarus* 106, 228–246), to account for the effects of strong tidal forces on accretion. Our findings indicate that tidally modified accretion occurs in a relatively broad range of orbital radii surrounding the classical Roche limit. Tidally modified accretion has a very unique character: for a given particle density, only bodies which differ greatly in mass can remain gravitationally bound, as like-sized bodies overflow their mutual Hill sphere. We find that this constraint greatly limits the degree of accretional growth and prevents runaway accretion near the Roche limit. Numerical simulations show that through the course of tidally modified accretion, a fragmentation-produced debris distribution evolves into a *bimodal* population, with one element consisting of a swarm of small, high-velocity bodies and the other composed of a small number of large "moonlets" on fairly circular orbits. The latter are precluded from accreting with one another due to the tidal influences of the planet. Tidally modified accretion thus offers a natural explanation for the formation of systems of coexisting rings and ringmoons from disrupted parent bodies.

I. INTRODUCTION

In the past decade, our growing knowledge of the outer planets has revealed complex systems of rings and satellites surrounding the gas giants, each with its own unique properties and intrigue. In each system we observe moons, dust, and ring particles all coexisting inside what has classically been defined as the "Roche limit." For a recent review, see Esposito (1993). One of the most fundamental questions concerning these systems is the nature of their origin. Early ring formation theories proposed that rings represent residual debris from the era of planet formation which remains dispersed because of the strong tidal forces of the host planet. Such theories continue to be challenged by more recent ring lifetime estimates that are much shorter than the age of the Solar System; current work supports a dynamic scenario for rings involving a continual source of ring material supplied through the erosion and disruption of nearby ringmoons and satellites. For example, Harris (1984) and Dones (1991) have proposed that rings are the result of the disruption of satellites and/or captured comets whose reaccumulation was precluded by the strong tidal forces of the planets. This seems to agree well with the fact that the known ring systems lay within the classical Roche limit. Additional recent works by Colwell and Esposito (1992, 1993) have numerically demonstrated that satellite fragmentation caused by meteoroid impact can lead to the formation of narrow rings through a "collisional cascade."

Although debris from satellite disruptions is commonly considered a source of planetary ring material, recently the questions of the possible reaccretion of fragmented satellite debris and of accretion within the Roche limit in general have been raised by several works. Simulations by Soter (1971) and Canup and Esposito (1992) have demonstrated that, in the absence of tidal forces, reaccretion of small disrupted satellites occurs on time scales as short as 10–100 years. Numerical N-body simulations by Salo (1992) predict rapid formation of meter-sized aggregates in Saturn's A ring. Although the very presence of planetary rings denies the dominance of rapid accretion, these works suggest that limited accretion may occur in the planetary ring environment.

Recently, Colwell and Esposito (1992, 1993) have demonstrated that many of the small moons of Uranus and Neptune have collisional lifetimes against estimated meteoroid impact much shorter than the age of the Solar Sys-

0019-1035/95 $6.00

tem, and it therefore is unlikely that these moons are primordial. If the existing moons are merely large fragments from earlier disruptions, Colwell and Esposito have shown that an unrealistically large initial moon population or a ring/satellite system which is currently near the end of its life is required to explain the current moon population. Limited reaccretion would be a possible answer to this dilemma.

Analysis of Saturn's G ring has shown that in addition to a large dust component, the ring also likely contains many moon-sized parent bodies with lifetimes against mutual collision much shorter than the age of the Solar System (Showalter and Cuzzi 1993). Showalter and Cuzzi propose that the band of G-ring parent bodies are the remaining fragments of an earlier disruption of a larger satellite. However, with this explanation alone, it is difficult to account for the bimodality of the current ring size distribution, since fragmentation events typically produce power-law debris size distributions. Additionally, it has been difficult to explain why the parent bodies have not reaccumulated into a single body, since the G ring is located outside the classical Roche limit.

The history of the inner Neptune satellite system is also suggestive of accretion inside the classical Roche limit. Banfield and Murray (1992) have proposed that the capture of Triton imparted large eccentricities to the precapture interior satellites of Neptune, causing them to occupy highly crossing orbits. They hypothesize that any original satellites would be quickly destroyed through mutual collisions and that the existence of the current inner satellites is due to the accretion of an equatorial disk of collisional debris. While this seems to account for the nearly equatorial orbits of the inner satellites, four of these satellites are located within the Roche limit.

Thus, while fragmentation plays a crucial role in the origin and evolution of ring and satellite systems, competing accumulation processes may also be important. Between the orbital regime of the inner ring systems (where tidal forces certainly preclude significant accretion) and outer regular satellite systems (where accretion proceeds rapidly) is a transitional realm. The aforementioned works support a more thorough investigation of tidally influenced accretion in the interest of better understanding the origin and evolution of rings and moons observed near the Roche limit.

The main body of work investigating the accretion process has been conducted in the context of the accretion of planets about the Sun. Several extensive numerical simulations (e.g., Greenberg *et al.* 1978, Spaute *et al.* 1991, and Wetherill and Stewart 1989, 1993) have been developed to model the accretion of the planets, which occurred far outside the Sun's Roche limit, at ~ 80–$6000 R_{\odot}$. These simulations have made great strides in the study of the mass and velocity evolution of colliding swarms of orbiting bodies, and our work utilizes many of their advances. However, planetary accretion simulations ignore tidal forces and use two-body approximations to model collisional events. Many of these approximations are invalid in a tidal environment, where three-body gravitational effects are significant.

The nature of the effects of tidal forces on accretion in planetary rings has been previously examined in Weidenschilling *et al.* (1984) and Longaretti (1989). This work represents an extension of the study of such tidal effects by these works and detailed comparisons are made in Section V.A.

The goal of this work has been to develop a numerical model for accretion valid in the planetary ring environment which accounts for the competing tidal forces of the host planet in a more self-consistent and complete manner than has been done previously. We examine the effects of accretional processes in the Roche zone for centimeter- to kilometer-sized bodies. Our results indicate that: (1) tidal forces affect accretion in a range of orbital radii surrounding the classical Roche limit, (2) accretion under the influence of tidal forces has a general character much different from that of accretion far away from the primary, and (3) tidally modified accretion offers a natural explanation for the coexistence of moonlets and ring material. Section II (as well as Appendices A and B) describes the details of our numerical model, Section III presents our numerical results, Section IV discusses an analytic estimate of steady-state populations, Section V compares our results to related previous work and discusses implications for specific ring/moon systems, and Section VI presents our general conclusions.

II. MODEL DESCRIPTION

Our approach is to simulate the mass and velocity evolution of a colliding swarm of particles with a discretized, probabilistic model spanning a broad distribution in size. While N-body simulations (see Salo 1992, Ohtsuki 1993) follow individual particles, we calculate average collision rates for binned intervals of a continuous mass distribution. These rates determine the mass and kinetic energy evolution of the swarm through accretion, avoiding severe computing constraints on the number of bodies that can be considered.

We model the evolution as a time-dependent Markov process. A Markov process is a stochastic process without memory; the evolution of a Markov system at any time depends only on the state of the system at that time and not on the history of how the state was achieved. The evolution of a Markov system is described by probabilities for transition between all possible states of the system; if these probabilities evolve with time, the process is called "time-dependent." In general, the Markov formalism is

a natural means for describing the evolution of systems driven by probabilistic random events. In our model, the "states" for the accreting material of this stochastic system are the bins in mass which span the size distribution of the accreting objects. At an initial time a vector describes the distribution of the total mass among these size bins. For each time step we calculate the probabilities of mass transfer from one bin to another by an accretional collision. The set of these probabilities for the given time interval forms a "transition matrix" for transfers among the states of the system. Multiplication of the present vector by this matrix yields the expectation values of the size distribution after one time step.

Previous accretion codes have computed mass transfer rates between mass bins. By adopting a Markov approach, we have in effect translated these rates into probabilities for mass transfer. Our method tracks *expectation values;* these may differ from actual realizations if the number of objects is small. Our approach offers an organized, easy to understand algebraic structure and allows us to readily examine the likelihood of accumulation for a range of masses. Additionally, the Markov approach allows us to easily prohibit unphysical collisions (such as those which would lead to the formation of a body with a mass greater than the total mass) and to rigorously conserve mass. Thus our simulation avoids many of the defects of purely statistical treatments of accretional growth which have recently been discussed by Tanaka and Nakazawa (1994).

A. Mass Evolution

This model considers only particle growth through accretionary processes. Fragmentation and erosion processes are ignored. In general, collisions in and near ring systems will occur with impact velocities in the cm/sec to m/sec range, too small to fragment competent natural objects. However, loosely accumulated material may be knocked off during nonaccreting collisions, and some production of debris via erosion is likely to occur. A more extensive discussion of this matter is contained in Section IV.

1. Representation of the population. The evolution of the mass distribution of a population of accreting bodies can be described by the coagulation equation. The integrodifferential form of the coagulation equation is

$$\frac{d}{dt}n_m = \frac{1}{2}\int_0^m n_{m'}n_{m-m'}A_{m',m-m'}\,dm' - n_m\int_0^\infty n_{m'}A_{m,m'}A_{m,m'}\,dm', \tag{1}$$

where $n_m dm$ represents the number of bodies with mass between m and $m + dm$ and $A_{m',m-m'}$ is the probability that a collision resulting in accretion between mass m' and mass $(m - m')$ particles occurs per unit time (e.g., Wetherill 1990). The first integral represents the formation of mass m particles through collisions involving mass m' and $(m - m')$ particles. The factor of 1/2 ensures that the same collisions are not counted twice. The second integral represents the loss of mass m particles as they collide and accrete with all other particles.

We model the integrodifferential coagulation equation using a Markov process matrix representation, consisting of a time-evolving state vector, S, and a transition matrix, T. The state vector describes the logarithmic mass distribution of a system of particles at a given time. The kth element of this state vector is the total mass contained in particles whose mass lies between $2^k M_0$ and $2^{k+1}M_0$, where M_0 is an arbitrary unit mass. If M_k is defined as the total amount of mass in the kth bin of S, then M_k is given by

$$M_k = \int_{m_k}^{m_{k+1}} m' n_{m'} dm', \tag{2}$$

where m_k and m_{k+1} are the lower and upper mass limits, respectively, of the kth bin, and n_m is the mass distribution across the bin. We define n_m to be a differential power law of the form

$$n_m dm \propto m^{-q_m} dm, \tag{3}$$

where q_m is the mass differential exponent. We compute both collision probabilities and mass transfer between bins based on integration of this continuous mass distribution within each mass bin. The mass distribution for a nonfragmenting, accreting system has been shown to asymptote to $q_m \approx 1.55 \pm .15$ for all but the largest bodies in a system, whose mass distribution is characteristically much shallower (Zvyagina and Safronov 1972). With this in mind we have chosen $q_m = 1$ for all mass bins as a reasonable approximation; this choice has the added benefit of simplifying many of the collisional integrals described in Appendix A.

The final bin of our state vector is a discrete mass bin, which describes particles whose mass equals that of the total amount of mass in the simulation, M_{tot}. If our state vector contains Y mass bins, then the expectation value of the number of bodies in bin Y, N_Y, is always a number between 0 and 1. If all the mass in a simulation were to accrete into a single body, N_Y would equal exactly one. Mass contained in the final bin does not collide with itself or with mass contained in any other mass bin, since in a real system the last bin contains a body only when all other bins are empty.

The transition matrix, T, regulates mass transfer between bins of the state vector. The (i, k) element of the transition matrix, $T(i, k)$, is the probability that a unit mass will be transferred from bin i to bin k in one time

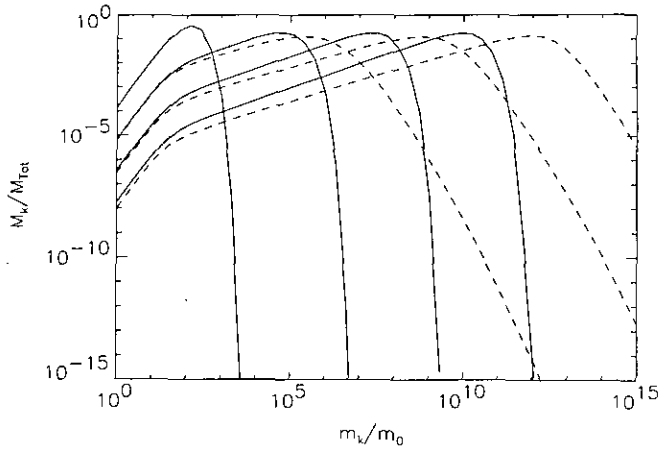

FIG. 1. Comparison of analytic (solid) and numerical (dashed) solutions to the coagulation equation for $A_{m,m'} \propto \beta(m + m')$ at four stages: $\eta = 0$, 3, 6, and 9. Here η is a dimensionless time defined as $\beta t m_T$, where β is the collision frequency, t is time, m_T is the total amount of mass in the system. Plotted on the x axis is the lower limit of the mass bin divided by the smallest mass in the simulation; the y axis gives the total mass of particles found in the bin normalized by the total amount of mass in the system.

step as a result of accretion. Accordingly, $T(k, k)$ is the probability that mass in the kth mass bin will remain in the kth bin during one time step. The transition matrix elements are derived in Appendix A. The evolution of the system of particles through one time step is found by multiplication of the transition matrix by the state vector. Time step sizes are adjusted so that no more than 10% of the mass contained in any mass bin experiences a collision during one time step. This ensures that during a single time step particles are unlikely to undergo more than one collision and that the state vector will not change enough during a time step to significantly affect the transition probabilities computed for that time step.

Our state vector thus describes the stochastic evolution of the logarithmic mass distribution of a system of particles at a given time. The kth element of the state vector represents the amount of mass contained in particles ranging in mass from m_k to $2m_k$. Since $S(k)$ is an expectation value, it is equivalent to the average amount of mass in this range that would be calculated from a large number of Monte Carlo simulations (see Kemeny and Snell 1960, Esposito and House 1978).

2. Comparison with analytic results. The coagulation equation is analytically solvable for several forms of the collisional cross section, $A_{m,m'}$. Figure 1 compares our Markov process formalism of the coagulation equation to analytical results for the "sum-of-the-masses" case, with $A_{m,m'} = \beta(m + m')$, where β is a constant. The initial condition for this simulation is a steeply peaked exponential distribution given by

$$\frac{dn}{dm} = \frac{n_0}{m_0} e^{-(m/m_0)}, \tag{4a}$$

where n_0 is the initial number of particles and m_0 is the average initial mass (Safronov 1963). The discretized initial mass distribution for our Markov method is obtained by integrating Eq. (4a) over the width of each mass bin. The analytic solution to Eq. (4a) is (Safronov 1963)

$$n(m, \eta) = \frac{n_0 g e^{-m/m_0(1-\sqrt{1-g})^2}}{2\sqrt{\pi}(m/m_0)^{3/2}(1-g)^{3/4}}, \tag{4b}$$

where η is the dimensionless time defined as

$$\eta = \beta m_T t, \tag{4c}$$

where m_T is the total amount of mass, and g is the fraction of bodies remaining at a given time t. Figure 1 is plotted in a format similiar to comparisons done by Ohtsuki *et al.* (1990) and Wetherill (1990). When compared to analytical results, our numerical results show an "artificial acceleration" of accretional growth, a well-documented trait of simulations using logarithmically spaced fixed mass bins (see Ohtsuki *et al.* 1990, Wetherill 1990). Our agreement with analytic results is slightly better than that found by Ohtsuki *et al.* (1990) for a comparable bin spacing; this is due to the fact that we integrate over the mass distribution in each mass bin instead of simply assigning a mean arithmetic mass to each bin. However, we still experience considerable acceleration, since mass which enters a bin is distributed by our simulation across the entire bin width with a relatively shallow distribution. The problems of artificial acceleration have been largely solved by both the Wetherill and Stewart (1989, 1993) and the Spaute *et al.* (1991) models; the former utilizes adjustable bin widths while the latter considers a variable slope for the mass distribution in each bin based on the population in neighboring bins. Both models require far more complicated numerical treatments than the approach used in this work. Despite the spurious acceleration of accretional growth that is associated with our fixed-bin system, our numerical results demonstrate that neither complete reaccumulation nor runaway accretion occur in a tidal environment (see below). Adopting a more accurate and complex approach such as those of Wetherill and Stewart or Spaute *et al.* would only strengthen this basic conclusion. With this in mind, we restrict our attention to more general statements about accretion outcomes.

3. Collision frequency determination. Approaches for determining collision frequencies range from explicit orbit integration for few-body systems to averaging schemes for many-body systems. We have used a "particle-in-a-box" (hereafter PIAB) approximation to estimate colli-

sion probabilities between debris particles; this approximation and many derivatives thereof have been widely used in accretion simulations (e.g. Greenberg *et al.* 1978, Spaute *et al.* 1991, Wetherill and Stewart 1989, 1993, Weidenschilling *et al.* 1984). The PIAB approach assumes that within a "box" traveling on a circular orbit about a primary, a system can be treated as an ideal gas whose particles have relative velocities which are determined by the particles' random motion. This random motion can be described by a particle's radial and vertical epicyclic excursions from local mean circular motion, given by

$$v_{\rm ran} = a\Omega\sqrt{\frac{5}{8}e^2 + \frac{1}{2}i^2}, \tag{5}$$

where a is the orbital semimajor axis, Ω is the orbital frequency, and e and i are the orbital eccentricity and inclination (Lissauer and Stewart 1993). Equation (5) assumes the epicyclic approximation, that is $e, i \ll 1$. In the PIAB approximation, each particle is assumed to encounter a proportionally representative sample of the population of the swarm during a time step.

The PIAB approximation is valid when encounter velocities are determined by random motion and the effects of Keplerian shear are negligible. Numerical N-body simulations (e.g., Petit and Henon 1986) and analytic work (Greenberg *et al.* 1991) have shown that the PIAB collision rates are valid when the relative velocity of colliding particles due to their random motion is greater than about twice the shear velocity across their mutual Hill sphere. The radius of the mutual Hill sphere of two bodies is given by

$$R_{\rm Hill} = a\left(\frac{m + m'}{3M_{\rm plan}}\right)^{1/3}, \tag{6}$$

where $M_{\rm plan}$ is the mass of the planet (Nakazawa and Ida 1988). A "Hill velocity" can be defined as $v_{\rm Hill} = \Omega R_{\rm Hill}$. We consider the PIAB approximation to be valid when

$$v_{\rm rel} > 2.17 v_{\rm Hill}, \tag{7}$$

where $v_{\rm rel}$ is relative encounter velocity due to random motion. Equation (7) is equivalent to the Greenberg *et al.* (1991) Eq. (11).

Using the PIAB representation, the probability that two particles of mass m and m' will collide and accrete per unit time is

$$A_{m,m'} = \frac{\alpha\sigma_{m,m'}v_{\rm rel}}{2\pi aWH}, \tag{8}$$

where α is the probability that the collision will result in accretion, $\sigma_{m,m'}$ is the collisional cross section, and W and H are the mutual scale width and height of the "box" occupied by the particles.

We use a geometric cross section enhanced by two-body gravitational focusing as our collisional cross section,

$$\sigma_{m,m'} = \left(\frac{3}{4}\right)^{2/3}\pi^{1/3}\rho^{-2/3}(m^{1/3} + m'^{1/3})^2\left(1 + \frac{v_{\rm esc}^2}{v_{\rm rel}^2}\right), \tag{9}$$

where ρ is the particle density and $v_{\rm esc}$ is the mutual escape velocity of the colliding particles (e.g., Greenberg *et al.* 1991). The two-body gravitational focusing expression agrees well with numerical N-body simulations for the range of velocities over which the PIAB approximation is valid (see Greenzweig and Lissauer 1990, Fig. 8a). We assume that particles collide at random orientations, so that their relative velocity is given by

$$v_{\rm rel} = (v_{\rm ran}^2 + v_{\rm ran}'^2)^{1/2} \tag{10}$$

We also assume an isotropic dispersion of $v_{\rm ran}$, so that the mutual scale height and width for two particles are given by

$$H \sim W \sim \frac{1}{\Omega}(v_{\rm ran}^2 + v_{\rm ran}'^2)^{1/2} \tag{11}$$

(Stewart *et al.* 1984). The determination of α is described in Section II.C.

B. Velocity Evolution

In addition to following the mass evolution of the swarm, we also track velocity evolution. The particles in each mass bin are assigned a mean kinetic energy, $\langle v_{\rm ran}^2\rangle$, which evolves with time as a result of physical collisions and gravitational encounters. We utilize the work of Stewart and Wetherill (1988) to account for the change in random velocity which a given mass bin experiences per unit time as a result of viscous stirring due to gravitational encounters, viscous stirring due to inelastic collisions, energy damping due to inelastic collisions, and energy exchange due to dynamical friction (their Eqs. (9a)–(9d)). Stewart and Wetherill adopted two-body approximations to derive their velocity evolution expressions for gravitational encounters. In a tidal regime, the range of impact parameter over which such approximations are appropriate is much smaller than in typical planetary accretion scenarios. As bodies fill an appreciable volume of their Hill sphere, physical collisions become more likely than scatterings during close encounters (Canup *et al.* 1993). Consequently, velocity evolution in a tidal regime is typi-

cally dominated by the effects of collisions. In the Stewart and Wetherill formalism, the magnitude of velocity evolution due to viscous stirring and dynamical friction is proportional to ln Λ, where Λ is approximately the ratio of the maximum scale height of the interacting bodies to their collisional cross section. In a tidal environment, the scale height is often not much larger than the Hill radius, and Λ approaches 1. More distant encounters, neglected by the Stewart and Wetherill treatment, will be more significant in a tidal environment than they are for orbits far outside the Roche radius of the primary. We adopt the Stewart and Wetherill expressions as first-order approximations.

We have compared velocity distributions obtained with our model to steady-state distributions obtained from the Stewart and Wetherill (1988) equations for several different power law mass distributions, and find good agreement for the case of a nonaccreting swarm at 1 AU from the Sun (see Lissauer and Stewart 1993, Fig. 1). In addition to the Stewart and Wetherill (1988) considerations, we have included velocity evolution due to accretion in a manner consistent with their approach (see Appendix B). We assume that accreting impacts are completely inelastic, and each accreting pair of bodies is assigned a random velocity equal to the center of mass velocity of the two bodies prior to impact, given by

$$v_{cm} = \left(\frac{v_{ran}^2 m^2 + v'_{ran} m'^2}{(m + m')^2}\right)^{1/2} \tag{12}$$

(Ohtsuki 1992). The rms velocity of the mass bin where the newly accreted particle is placed is adjusted according to Eq. (B5) in Appendix B.

The particles described by a given mass bin will, in reality, exhibit a distribution of velocities. Greenzweig and Lissauer (1992) have shown that approximating such a distribution by a single rms velocity results in the underestimation of collision rates by a factor of ~3. Since we are more concerned with the mass distribution produced than the exact length of time taken to produce it, a single velocity per mass bin is adequate for our purposes.

C. Accretion Criteria

Previous accretion simulations have utilized a simple two-body approximation to determine when collisions result in accretion. In free space, two bodies that collide will remain gravitationally bound if their rebound velocity is less than their mutual escape velocity,

$$\begin{aligned} v_{reb} &< v_{esc} \\ v_{reb} &= \varepsilon v_{imp}, \end{aligned} \tag{13}$$

where v_{reb} is the relative rebound velocity, v_{imp} is the relative impact velocity, and ε is the coefficient of restitution. In the two-body approximation, the impact velocity is given by

$$v_{imp}^2 = v_{rel}^2 + v_{esc}^2, \tag{14}$$

where v_{rel} is the relative velocity of the particles at infinite separation. Equations (13) and (14) yield the capture criterion used by Greenberg *et al.* (1978), Spaute *et al.* (1991), Wetherill and Stewart (1989, 1993), and Weidenschilling *et al.* (1984):

$$\varepsilon < \varepsilon_{crit,2B} \equiv \sqrt{\frac{v_{esc}^2}{v_{esc}^2 + v_{rel}^2}}. \tag{15}$$

Equation (15) defines a critical maximum value of the coefficient of restitution, $\varepsilon_{crit,2B}$ for accretion.

While the two-body capture criterion is well suited for accretion far outside the Roche limit, it is not valid in tidal environments. In order to better model accretion in the Roche zone, we have implemented "three-body" capture criteria after the work of Ohtsuki (1993), as described below. Previous works which have examined the effects of tidal influences on accretion (Longaretti 1989 and Weidenschilling *et al.* 1984) have adopted a "force" approach, defining a range of orbital radii over which two bodies initially in contact and at relative rest will experience a net attractive force. Here, we derive tidal capture criteria from an *energy* perspective, considering both relative kinetic and potential energies in a three-body formulation.

The relative motion of two bodies in orbit about a primary can be described by the Hill approximation, in which the motion of orbiting bodies is described relative to a coordinate system rotating on a Keplerian circular orbit. In this coordinate system, the x axis points radially outward, the y axis points tangent to the circular orbit, and the z axis is normal to the orbital plane. Typically, Hill's equations are written in nondimensionalized form, with time scaled by Ω^{-1} and length scaled by R_{Hill}; velocities are correspondingly in units of v_{Hill}. The linearized equations of relative motion are

$$\begin{aligned} \ddot{x} &= 2\dot{y} + 3x - 3x/r^3 \\ \ddot{y} &= -2\dot{x} - 3y/r^3 \\ \ddot{z} &= -z - 3z/r^3, \end{aligned} \tag{16}$$

where x, y, and z are the relative coordinates in the rotating frame and $r = (x^2 + y^2 + z^2)^{1/2}$ (Nakazawa and Ida 1988). Equations (16) preserve the energy integral, often called the Jacobi integral,

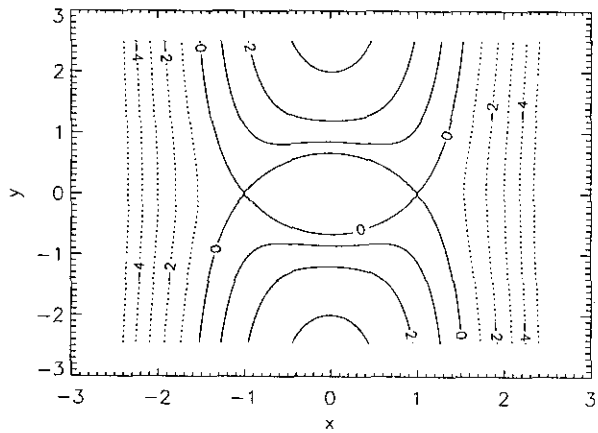

FIG. 2. The Hill potential for the $z = 0$ plane; units are in Hill units.

$$E = \frac{1}{2}(\dot{x}^2 + \dot{y}^2 + \dot{z}^2) + U(x, y, z), \tag{17}$$

where $U(x, y, z)$ is the Hill potential:

$$U(x, y, z) = -\frac{3}{2}x^2 + \frac{1}{2}z^2 - \frac{3}{r} + \frac{9}{2}. \tag{18}$$

Here E represents the total energy in the rotating frame. The first two terms of U account for the tidal potential, the third represents the mutual gravity between the orbiting objects, and the constant 9/2 has been added so that U vanishes at the Lagrangian points, $(x, y, z) = (\pm 1, 0, 0)$ (Nakazawa and Ida 1988). Figure 2 shows the Hill potential in the $z = 0$ plane. The $U = 0$ contour line defines the Hill "sphere," which is actually lemon-shaped with a half-width of $R_{\rm Hill}$ in the radial direction, $2/3R_{\rm Hill}$ in the azimuthal direction, and $\approx 0.64\ R_{\rm Hill}$ in the vertical direction. Since the $U = 0$ contour line is closed, two objects cannot escape from their mutual Hill sphere if their total relative energy (given by Eq. (17)) is negative after their collision (Ohtsuki 1993). This condition can be used to derive a three-body capture criterion.

When two orbiting bodies are far apart ($r = \infty$) the Jacobi integral associated with their motion can be expressed in terms of their instantaneous relative orbital elements,

$$E_\infty = \frac{1}{2}(e_{\rm H}^2 + i_{\rm H}^2) - \frac{3}{8}b^2 + \frac{9}{2}, \tag{19}$$

where $e_{\rm H}$ and $i_{\rm H}$ are the Hill eccentricity and inclination, respectively, and b is the scaled separation in semimajor axis (Ohtsuki 1993). Immediately before the two bodies collide, E is still given by E_∞,

$$E = E_\infty = \frac{1}{2}v_{\rm i}^2 - \frac{3}{2}x_{\rm p}^2 + \frac{1}{2}z_{\rm p}^2 - \frac{3}{r_{\rm p}} + \frac{9}{2}, \tag{20}$$

where $v_{\rm i}$ is the scaled impact velocity, $r_{\rm p}$ is the scaled sum of the particles radii,

$$r_{\rm p} = (r + r')/R_{\rm Hill}, \tag{21}$$

and $x_{\rm p}$, $y_{\rm p}$, and $z_{\rm p}$ are the coordinates of the impact point, such that $x_{\rm p}^2 + y_{\rm p}^2 + z_{\rm p}^2 = r_{\rm p}^2$ (Ohtsuki 1993). Equation (21) can also be expressed as

$$r_{\rm p} = \frac{R_{\rm p}}{a}3^{1/3}\left(\frac{\rho}{\rho_{\rm p}}\right)^{-1/3}\frac{1 + \mu^{1/3}}{(1 + \mu)^{1/3}}, \tag{22}$$

where $R_{\rm p}$ and $\rho_{\rm p}$ are the radius and density of the planet, and μ is the mass ratio of the colliding objects, where $0 < \mu < 1$ (Ohtsuki 1993).

At this point we deviate from Ohtsuki (1993), who neglects the two tidal terms in Eq. (20), as we consider the full three-body potential. If two bodies collide with random orientation, averaging Eq. (20) over all orientations gives their average relative scaled velocity upon impact:

$$v_{\rm i}^2 = 2E_\infty + 6/r_{\rm p} + \frac{2}{3}r_{\rm p}^2 - 9. \tag{23}$$

In following with Ohtsuki's (1993) notation we define

$$v_{\rm e}^2 = 6/r_{\rm p}, \tag{24}$$

where $v_{\rm e}$ is the scaled mutual escape velocity and

$$v_{\rm b}^2 = (e_{\rm H}^2 + i_{\rm H}^2) - \frac{3}{4}b^2, \tag{25}$$

where $v_{\rm b}$ is the relative velocity at $(x, y, z) = (0, 0, 0)$ in the unperturbed (neglecting mutual gravity) solution to Eqs. (16). For the PIAB regime, random motions dominate over motion due to Keplerian shear and $v_{\rm b}^2$ is positive. From Eqs. (13), (19), and (23)–(25) the scaled rebound velocity is given by

$$v_{\rm r} = \varepsilon\left[v_{\rm b}^2 + v_{\rm e}^2 + \frac{2}{3}r_{\rm p}^2\right]^{1/2}. \tag{26}$$

We have defined ε to represent the net reduction of relative velocity due to the inelasticity of an impact. It is related to the normal and tangential coefficients of restitution, $\varepsilon_{\rm n}$ and $\varepsilon_{\rm t}$, respectively, by

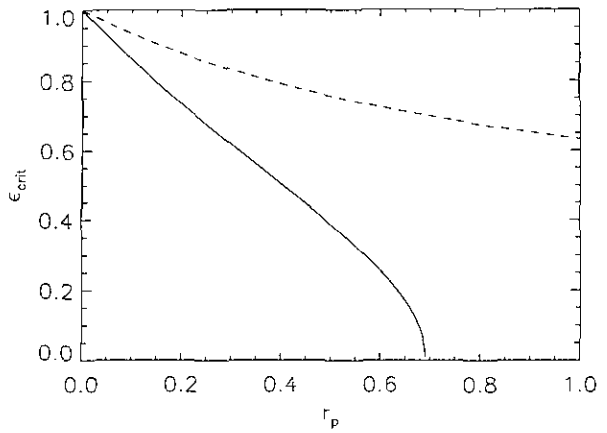

FIG. 3. The critical coefficient of restitution for accretion as a function of the scaled size of a colliding particle pair ($r_p = (r + r')/R_{Hill}$), using the standard two-body approximation (dashed) and the three-body approach (solid). For collsions between like-sized objects of a given density, r_p varies inversely with orbital radius. For a collision to result in gravitational accretion, ε must be less than ε_{crit}.

$$\varepsilon = \left[\frac{\varepsilon_n^2 v_n^2 + \varepsilon_t^2 v_t^2}{v_n^2 + v_t^2}\right]^{1/2}, \tag{27}$$

where v_n and v_t are respectively the normal and tangential components of the relative impact velocity. This definition of ε_t, used by Ohtsuki (1993), differs from that of Araki and Tremaine (1986) and Longaretti (1989), who defined ε_t as the change of the relative velocity between the points of contact of colliding objects. From Eqs. (17), (18), and (26), the total energy after the collision is then

$$E' = \frac{1}{2}\varepsilon^2\left(v_b^2 + v_e^2 + \frac{2}{3}r_p^2\right) - \frac{3}{r_p} - \frac{1}{3}r_p^2 + \frac{9}{2}, \tag{28}$$

If the collision is inelastic enough so that the total energy after the collision is less than zero, the bodies cannot escape their mutual Hill sphere. This $E' < 0$ condition defines a critical coefficient of restitution from Eq. (28):

$$\varepsilon < \varepsilon_{crit,3B} = \sqrt{\frac{v_e^2 + (2/3)r_p^2 - 9}{v_e^2 + v_b^2 + (2/3)r_p^2}}. \tag{29}$$

The specific choice of impact orientation determines the coefficient of the r_p^2 term; here we have assumed random impact orientation. The r_p^2 coefficient is 3 in the case of impacts occurring in the radial direction, -1 for impacts in the vertical direction, and 0 for impacts oriented in an azimuthal direction. Figure 3 shows a comparison of $\varepsilon_{crit,2B}$ (given by Eq. (15)) and $\varepsilon_{crit,3B}$ for a single value of v_b as a function of r_p. In planetary accretion scenarios, r_p is typically of order 10^{-3}–10^{-2} for collisions of like-sized bodies, and the two-body approximation is reasonable. As r_p becomes appreciable, as is the case in the Roche zone, the three-body approach is required.

The definition of $\varepsilon_{crit,3B}$ yields two requirements for capture. First, in order for Eq. (29) to be satisfied, $\varepsilon_{crit,3B}$ must be greater than or equal to zero, so that

$$6/r_p + \frac{2}{3}r_p^2 - 9 \geq 0, \tag{30}$$

or

$$r_p \lesssim 0.691. \tag{31}$$

Second, if Eq. (31) is satisfied, two bodies will remain within their mutual Hill sphere if ε is less than $\varepsilon_{crit,3B}$. In our model, we consider a coefficient of restitution which is independent of velocity and mass, and particle pairs which satisfy both Eqs. (29) and (31) are assumed to gravitationally accrete through successive inelastic mutual collisions.

Note that when the physical size of colliding bodies exceeds about 70% of their mutual Hill radius they will not on average remain gravitationally bound, *even if their collision is completely inelastic*. This differs markedly from the two-body approximation, where completely inelastic collisions always result in accretion. Equation (31) is also a more stringent requirement than that obtained using a force approach to model escape in the radial direction, which yields an $r_p < 1$ criterion (e.g., Longaretti 1989, Eq. 30). This is somewhat surprising since the Hill potential reaches a maximum only as one moves radially away from the origin. However, escape from the Hill sphere is also possible azimuthally and vertically, as motion in the rotating frame tends to follow isopotential lines, and the Hill "sphere" is actually narrower in these directions. Equations (22) and (30) define a critical mass ratio for accretion for a completely inelastic collision as a function of orbital location and particle density,

$$\frac{(1 + \mu_{crit})^{1/3}}{1 + \mu_{crit}^{1/3}} = \left(\frac{1}{0.691}\right) 3^{1/3} \frac{R_p}{a}\left(\frac{\rho}{\rho_p}\right)^{-1/3}, \tag{32}$$

where μ_{crit} is the maximum mass ratio that two bodies can have in order to remain gravitationally bound after a completely inelastic collision. In the limit of $\mu = 0$, Eq. (32) takes a form similar to that of the classical Roche limit:

$$\frac{a}{R_p} \simeq 2.09\left(\frac{\rho}{\rho_p}\right)^{-1/3}. \tag{32a}$$

The coefficient in Eq. (32a) is smaller than the coefficient

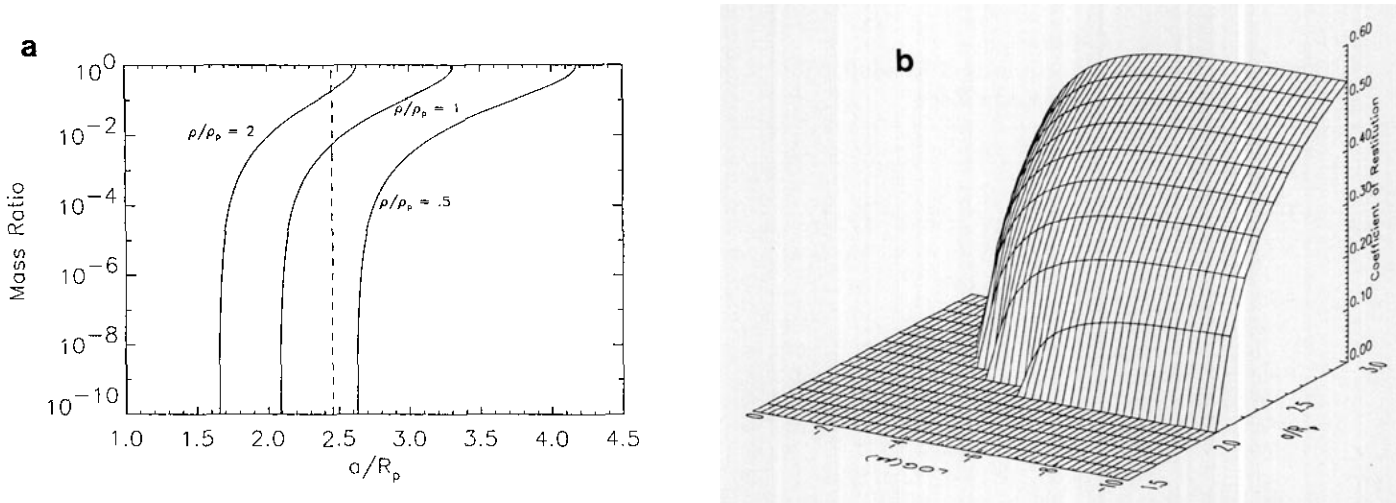

FIG. 4. (a) Critical mass ratios for accretion as a function of scaled orbital radius and particle density for completely inelastic collisions ($\varepsilon = 0$). Here ρ/ρ_p is the ratio of particle to planetary density. Accretion is possible to the left of the appropriate mass ratio curve. The classical Roche limit for a fluid body with $\rho/\rho_p = 1$ is indicated by the dashed line. (b) Critical coefficient of restitution for accretion surface as a function of mass ratio (μ) and scaled orbital radius for $\rho/\rho_p = 1$. Accretion is possible only for those values where the plotted function is nonzero.

in the classical Roche limit for liquid bodies (2.456) since here we have considered solid, nondeformable bodies. Equation (32a) defines a minimum critical density for solid body accretion, analogous to the critical "Roche density" for fluid bodies:

$$\rho_{crit} \approx 9.1 \left(\frac{R_p}{a}\right)^3 \rho_p. \tag{32b}$$

Values for ρ_{crit} range from 0.54 g/cm^3 at the outer A ring to 2.3 g/cm^3 in the middle of the C ring. These values are larger than those derived by Longaretti (1989, his Eq. (30)).

Figure 4a is a plot of the critical mass ratios for accretion as a function of particle density and orbital radius, with the classical Roche limit shown for comparison. The critical accretion curves in Fig. 4a were derived assuming random impact orientation; a choice of a specific impact orientation (e.g., a radial impact) shifts the curves slightly along the x axis but does not change their form. Note that like-sized ($\mu = 1$) bodies are precluded from accreting in a region that extends well beyond the classical Roche limit, while low mass ratio pairs can accrete interior to this limit.

The three-body critical coefficient of restitution also differs from its two-body analog in the limiting case of zero relative velocity between the colliding objects. In the two-body case, if $v_{rel} = 0$, the critical coefficient of restitution is one. In the three-body case, relative velocities upon impact will typically be nonzero even for circular orbits, due to the shear in Keplerian velocities associated with small differences in semimajor axis. If we approximate lower limit of relative velocity in the PIAB regime as $v_b = 0$ then from Eq. (29),

$$\varepsilon_{crit,3B} = \sqrt{\frac{v_e^2 + (2/3)r_p^2 - 9}{v_e^2 + (2/3)r_p^2}}, \tag{33}$$

which is always less than one in a tidal environment. Figure 4b is a surface plot of $\varepsilon_{crit,3B}$ when $v_b = 0$ as a function of orbital radius and mass ratio for $\rho/\rho_p = 1$. Collisions which reside in the phase space above the surface of Fig. 4b will not typically result in accretion; those below the surface may result in accretion if the actual relative velocity of the colliding objects is low enough. The $\varepsilon = 0$ plane of Fig. 4b yields the critical mass ratio curve for $\rho/\rho_p = 1$ in Fig. 4a.

Table I lists maximum values for accretion of μ_{crit} and $\varepsilon_{crit,3B}$ for specific locations of planetary rings and satellites located in the Roche zone for several values of particle density. Note that even in outer regions where like-sized bodies can remain gravitationally bound, some degree of inelasticity is necessary in order for a collision to result in accretion.

Our analytic capture criteria compare well with numerical N-body results by Ohtsuki (1993). His Fig. 9 shows the orbit of a particle colliding with targets of size $r_p = 0.65$ and 0.75; the former leads to accretion after two impacts, while the latter results in escape after the first collision. Additionally, capture probabilities obtained from multiple N-body simulations decrease abruptly from the $r_p = 0.6$ to the $r_p = 0.7$ case (see Ohtsuki's Figs. 10 and 11). For the case of zero initial relative velocity and a coefficient of restitution between 0 and 0.5, capture

TABLE I
Critical Mass Ratios and Coefficients of Restitution for Accretion in the Roche Zone

Planet	Satellite or Ring	a/R_p	Particle Density (g/cc) 2.0 μ_{crit}, ϵ_{crit}	1.5 μ_{crit}, ϵ_{crit}	.9 μ_{crit}, ϵ_{crit}
Saturn	Outer B-Ring	1.95	.043, .51	.0097, .43	9.0e-6, .22
	A-Ring	2.02-	.069, .53	.018, .46	1.9e-4, .28
		2.27	.39,.60	.092, .55	.0069, .42
	Atlas	2.28	.44, .61	.099, .55	.0076, .42
	Prometheus	2.31	.64, .61	.12, .56	.0097, .43
	F-Ring	2.32	.79, .61	.12, .56	.010, .43
	Pandora	2.35	1, .62	.14, .57	.013, .45
	Epimetheus	2.51	1, .65	.44, .60	.036, .50
	Janus	2.51	1, .65	.44, .60	.036, .50
	G-Ring	2.75-	1, .69	1, .64	.12, .55
		2.88	1, .70	1, .67	.23, .59
Uranus	Cordelia	1.95	.00053, .25	0, 0	0, 0
	ϵ-Ring	1.95	.00053, .25	0, 0	0, 0
	Ophelia	2.10	.0045, .36	.00020, .25	0, 0
	Bianca	2.32	.027, .46	.0050, .38	0, 0
	Cressida	2.42	.048, .50	.011, .42	2.3e-5, .19
	Desdemona	2.45	.057, .51	.014, .43	6.9e-5, .21
	Juliet	2.52	.083, .53	.022, .46	.00035, .27
	Portia	2.59	.12, .54	.033, .48	.0010, .31
	Rosalind	2.73	.25, .58	.067, .52	.0042, .37
	Belinda	2.95	1, .62	.19, .56	.017, .45
	Puck	3.37	1, .67	1, .63	1, .54
Neptune	Naiad	1.94	0, 0	0, 0	0, 0
	Thalassa	2.02	4.0e-6, .19	0, 0	0, 0
	Despina	2.12	.00063, .28	0, 0	0, 0
	1989N2R	2.15	.0010, .30	0, 0	0, 0
	Galatea	2.50	.025, .46	.0014, .36	0, 0
	1989N1R	2.53	.029, .47	.0058, .38	0, 0
	Larissa	2.97	.27, .57	.070, .51	.0047, .37
	Proteus	4.75	1, .76	1, .73	1, .67

Note. The maximum values for the three-body critical coefficient of restitution (ϵ_{crit}) and the critical mass ratio (μ_{crit}) for accretion at various satellite and ring locations as a function of the density of the accreting material. Values were obtained assuming random collision orientation (see Section II.C for details). At a given location and density, accretion is very unlikely if the mass ratio (μ) of the colliding objects is greater than μ_{crit} *or* the coefficient of restitution (ε) is greater than ε_{crit}. If $\mu < \mu_{crit}$ *and* $\varepsilon < \varepsilon_{crit}$ accretion may occur, depending on the specific values of μ and ε and the initial relative velocity of the colliding particles.

probability drops from about 80% for an $r_p = 0.6$ collision to 40% for an $r_p = 0.7$ collision, to ~15–30% for an $r_p = 0.74$ collision (Ohtsuki, Fig. 10). Thus Eq. (31) seems a good approximation for relatively inelastic ($0 < \varepsilon < 0.5$) collisions. Ohtsuki also finds that for circular orbits and $r_p < 0.5$, most collisions result in accretion if $\varepsilon < 0.6$. Our Eq. (33) predicts accretion for $\varepsilon \lesssim 0.5$ and $r_p \lesssim 0.5$. For more elastic collisions, our capture criteria may define the limits of accretion less accurately. Ohtsuki's N-body simulations for circular orbits with $\varepsilon = 0.9$ show a decreasing capture probability as r_p ranges from 0.1 to 1.0, with near zero capture probabilities for $r_p \geq 0.7$ (see Ohtsuki's Fig. 8). Our Eqs. (31) and (33) imply zero capture probability in this case for $r_p > 0.15$. The discrepancies between our analytic criteria and Ohtsuki's (1993) capture probabilities for large ε are most likely due to our neglect of specific impact orientation, which plays a more significant part in determining whether accretion will occur for highly elastic collisions. The results presented in the following section are all for very inelastic collisions, where our capture criteria agrees well with N-body simulation results.

III. RESULTS

A. Interpretation of Numerical Results

As is true for all numerical simulations, the interpretation of our results merits careful consideration. Inherent in our statistical approach to accretion is the neglect of individual particle orbits; we also neglect differences in mass distribution within a given mass bin. An element of our mass state vector specifies only the total amount of mass contained in bodies whose mass falls within the boundaries of the corresponding mass bin. A mass distribution specified in one of our simulations therefore corresponds to a nearly infinite number of real systems, which differ in the specific orbital elements and phases of the orbiting bodies and in the exact way in which mass in a given bin is distributed among particles described by that bin. A given mass distribution generated by our model is best interpreted as equivalent to what one would obtain by averaging the mass distributions generated from an infinite number of corresponding N-body simulations.

B. Initial Debris Distributions

In order to simulate debris distributions produced by the fragmentation of small satellites, we generate initial mass distributions based on experimental results of Davis and Ryan (1990). These experiments have demonstrated that the debris mass distribution produced by a fragmentation is best described by a two-component power law whose cumulative slopes, b_1 and b_2, are a function of the mass of the largest fragment, f_1,

$$b_1 = \frac{0.47}{\sqrt{f_1}}, \qquad b_2 = \frac{0.18}{\sqrt{f_1}}. \tag{34}$$

The parameterizations for the generation of initial debris distributions described here are the same as those used by Colwell and Esposito (1992, 1993).

C. Numerical Simulation of Accretion at the Adams Ring

As a example of accretion in a highly tidal environment, we have simulated the evolution of the debris produced through the fragmentation of a 1-km-radius body at the

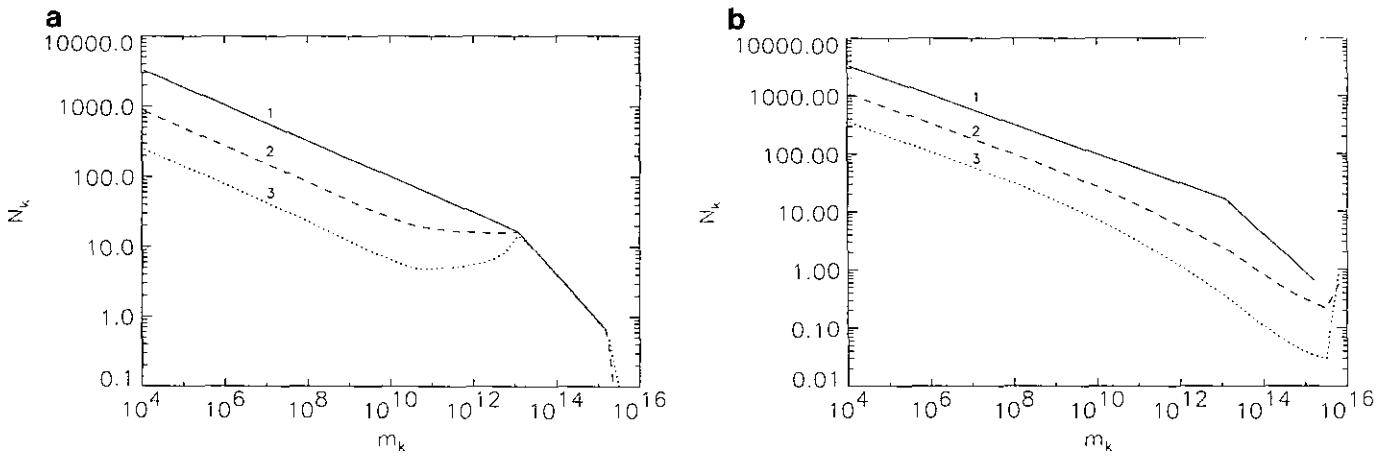

FIG. 5. The mass evolution of a debris swarm at Neptune's Adams Ring. Here $\rho = 1.5$ g/cm^3, $\varepsilon = 0.0$, and $v_{ran}(t = 0) = 560$ cm/sec. (a) Three-body tidal capture criteria. Mass distributions 1, 2, and 3 shown at $t = 0$, 300, and 600 years; m_k is shown in grams. (b) Two-body capture criterion. Mass distributions 1, 2, and 3 shown at $t = 0$, 500, and 3000 years.

orbit of Neptune's Adams ring, 1989N1R. Figure 5a shows the evolution of the mass distribution of objects larger than about 10 cm in radius using the tidal capture criteria described in Section II.C and $\varepsilon = 0$. Figure 5b shows the mass evolution using a standard two-body capture criterion. The initial mass distribution is the same for both cases. We have taken $f_1 = 0.5$, corresponding to initial mass differential slopes of $q_1 = 1.66$ and $q_2 = 1.25$, both shallower than the "equal mass per bin" $q_m = 2$ case. We have assumed the mass distribution within each mass bin has a differential slope $q_m = 1$ when deriving the number of bodies in the kth bin, N_k. All bins are initially assigned a random velocity of 560 cm/sec; this nominal value corresponds to an initial swarm width of 50 km, derived from numerical simulations of a 1-km satellite breakup at 1989N1R by Colwell and Esposito (1993). A particle density of 1.5 g/cm^3 is assumed.

Figure 5b demonstrates that when a two-body, $v_{reb} < v_{esc}$, criterion is used the satellite rapidly reaccretes; after 3000 years the probability that the satellite has reaccreted is near unity. This result is consistent with Soter (1971) and Canup and Esposito (1992). However, Fig. 5a shows that when the effects of tidal forces are included, the mass evolution has an entirely different character. Small bodies are depleted as they accrete onto bodies whose mass is much greater than their own ($\mu < 0.0058$ for accretion from Table I); the depletion rate of the small bodies as they accrete onto larger bodies is thus relatively insensitive to the mass of the small bodies, and the initial slope of the debris distribution is preserved. For bodies whose mass is greater than about 6×10^{11} g, the depletion rate decreases with increasing mass, as there are fewer bodies in the swarm large enough to satisfy the $\mu < \mu_{crit}$ accretion criterion. The largest initially occupied mass bins do not experience any significant change in occupation number; while they accrete smaller bodies, they are precluded from accreting with one another due to the influence of tides. The resulting mass distribution is *bimodal* in character, with a large number of centimeter-sized bodies and a few tens of 100-m to kilometer-radius bodies. The simulation was ended when velocities were low enough to make the PIAB collision rate invalid.

Velocity distribution evolution for the simulations described in Fig. 5 is shown in Fig. 6. Figure 6a is from the simulation using tidal capture criteria; Fig. 6b is from the simulation which used a two-body capture criterion. In general, random velocity decreases with particle size. In both cases, velocity evolution is dominated by the effects of collisions for bodies of mass $\gtrsim 10^{10}$ g. Typical values for Λ for collisions between large ($r \gtrsim 10$ m) bodies in the swarm are on the order of 1–100. For the simulation using the tidal capture criteria we find the largest fragments on nearly circular orbits, surrounded by a high velocity "swarm" of 10-cm to 10-m-radius bodies. The slight upturn in random velocity for the final two mass bins in Fig. 6a is in part due to the fact that the little mass which is found in these bins has entered the bins through collisions of smaller, high-velocity particles with bodies found in the third largest bin. The largest bins in this case also lack a population of larger bodies with which to rebound, which will tend to cause their rms bin velocities to be somewhat higher than smaller neighboring bins (conversely, in a stirring-dominated environment, such end effects will tend to lower the velocities of the largest bodies due to the absence of larger gravitational stirrers). In the simulation shown in Fig. 6b, mass enters the final two bins primarily through accretion between low-velocity objects found in the third largest bin (which is pre-

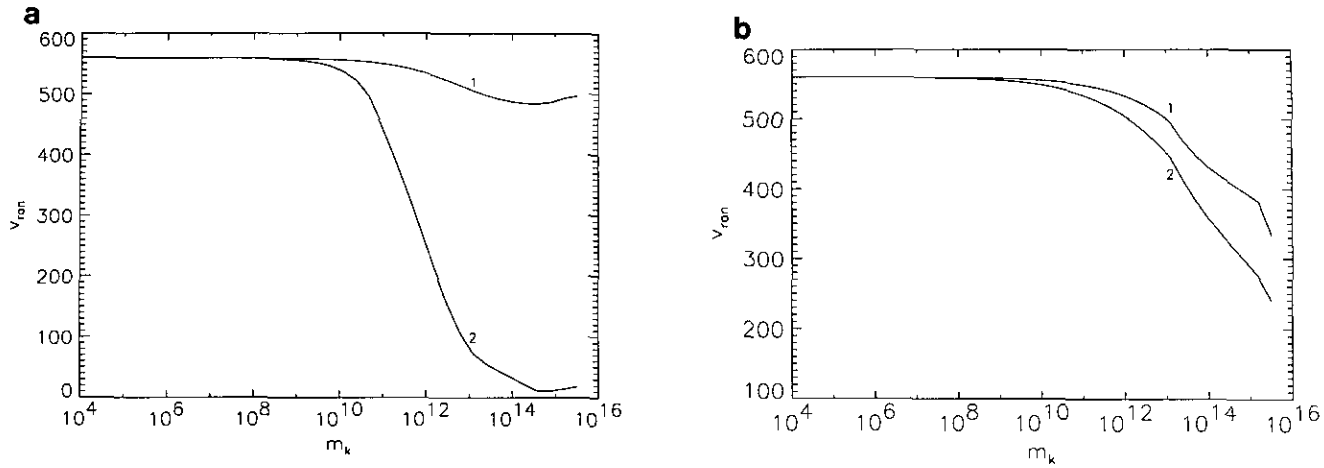

FIG. 6. Velocity distributions corresponding to the simulations shown in Fig. 5. All mass bins were initially assigned a random velocity of 560 cm/sec. (a) Velocity distributions 1 and 2 using the three-body tidal capture criteria at t = 100 and 600 years. (b) The same for the two-body capture criteria simulation at t = 500 and 3000 years.

cluded by the tidal capture criteria), leading to lower values of v_{ran} for the final two bins in this case. After ~500 years, velocity damping has had a much less significant effect in the simulation using the two-body capture criteria than for the simulation using the three-body capture criterion. Since we have considered completely inelastic collisions, a pair of bodies is assigned the same postimpact random velocity (v_{cm}) whether they rebound or accrete. However, in the two-body case, collisions lead to rapid accretional growth, producing larger bodies which are more effective gravitational "stirrers." In the three-body case, damping due to inelastic rebounding dominates and accretional growth of stirrers is limited.

Figure 7 shows the mass evolution for a 1-km moon disrupted again at 1989N1R, but here the mass of the largest initial fragment was taken to be about 6% of that of the original moon (f_1 = .0625), representing a highly catastrophic disruption. From Eq. (34), the initial distribution has differential power-law indices of q_1 = 2.88 and q_2 = 1.72; thus the high-mass leg of the initial distribution is steeper than the "equal mass per bin" case. Here again there is essentially no accretional growth of bodies larger than the largest initial fragment. Bodies contained in the largest 8 bins ($m_k \gtrsim 10^{13}$ g) are still unable to accrete with one another due to tidal constraints. The amount of mass in these bins increases more in this case than in the f_1 = 0.5 case because here there is a much greater amount of mass found in smaller particles which can accumulate onto the largest bodies. The bimodality of the final mass distribution is very prominent in this case, with a complete depletion of objects of ~10 m in radius (~5 × 10^9 g). The depletion is more extreme here than in Fig. 5a because of the very steep distribution of the largest bodies onto which the smaller bodies can accrete. The "bump" in the mass distribution for t = 100 years at ~4 × 10^{13} g is due to the accretion of the ~10-m bodies onto ~170-m bodies. Steep ($q_m \gtrsim 2$) mass distributions may thus lead to somewhat greater accretional growth of the largest bodies in a tidal environment, since they provide a proportionally greater number of smaller bodies with which the large bodies can accrete. However, even in the case of steep mass distributions, accretional growth of the largest bodies is very restrained by strong tidal effects.

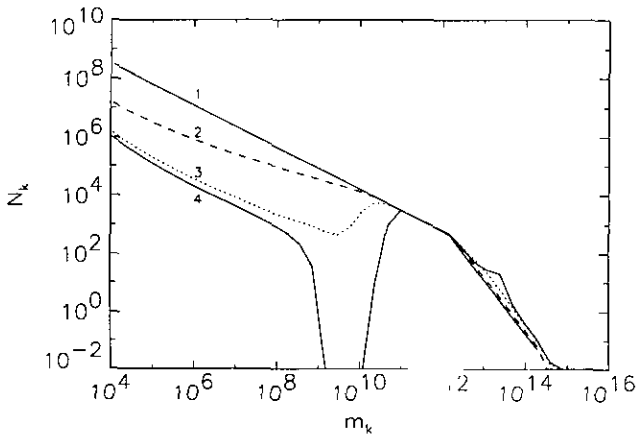

FIG. 7. The mass evolution of a debris swarm at 1989N1R. Same conditions as in Fig. 5a, except that here the mass fraction of the largest fragment was 0.0625, corresponding to a highly catastrophic disruption. Mass distributions 1–4 are shown for t = 0, 45, 90, and 100 years.

Mass distributions obtained for nonzero coefficients of restitution are similar to those shown in Figs. 5 and 7 if $\epsilon \lesssim 0.4$. In this case, all collisions rebound until velocities are damped to the order of the escape velocity of the largest objects. Accretion of low mass ratio bodies then

begins in the manner described above, with the difference that accretion among the smaller bodies in the swarm does not typically occur due to their higher relative (and thus higher rebound) velocities. For $\varepsilon > 0.38$, we find no accretion at 1989N1R for any 1.5 g/cm^3 density bodies. Table I may be used as a general guide for the upper limit of collisional elasticity which can lead to accretion at various ring and satellite locations.

Our results demonstrate that as a fragmentation-produced debris distribution undergoes tidally modified accretion it can evolve into a distribution with a bimodal character. Runaway accretion or reaccumulation of the original satellite is not observed. Figures 5a and 7 also show that in a tidal regime there exists a mass range of bodies over which the effects of accretion do not greatly change the character of the mass distribution. This range is a function of the mass of the largest body in the swarm, the particle density, and the distance from the planet and is approximately given by

$$m \gtrsim \mu_{\text{crit}} \times m_{\text{l}}, \tag{35}$$

where m_{l} is the mass of the largest fragment in the swarm and μ_{crit} is given by Eq. (32). The range may extend to somewhat lower masses than indicated by Eq. (35) for the case of highly catastrophic disruptions or when initial debris distributions are steeper than the equal mass per bin case. Thus, models of ring formation or of the disruption of satellites found in the Roche zone, such as those of Colwell and Esposito (1992 and 1993), may reasonably ignore accretion processes for the largest bodies in a swarm.

Tidal effects on accretion can also be understood in the context of their affect on the algebriac structure of a Markov chain. When all collisions in a closed system result in accretion, all mass will, theoretically, eventually accrete into a single body. In the Markov formalism this is represented by a Markov chain with a single *absorbing* state—the mass bin which describes objects whose mass is the total amount of mass in the system. Effectively, tidal effects on accretion result in the formation of multiple *absorbing* states, whose range is specific by Eq. (35) (Esposito and Canup 1993).

Our results combine well with those of Colwell and Esposito (1992, 1993) to suggest a possible origin scenario for narrow rings and related ringmoons. Parent satellites initially accumulate outside the Roche zone; those found at or within the corotation orbital radius tidally evolve inward toward the planet. Disruption by meteoroid impact will occur on time scales much shorter than 4.5 billion years (Colwell and Esposito 1992), and the debris produced will rapidly spread into a narrow ring due to phase mixing (Colwell and Esposito 1993). If the disruption occurs in the Roche zone, reaccretion of the debris will occur only between bodies which differ greatly in mass. This results in the formation of a bimodal mass distribution, consisting of a swarm of high-velocity small bodies and the largest initial fragments from the disruption. For highly catastrophic disruptions, the orbital specifics of the largest few objects might result in ring confinement, as in the case for the ε ring or 1989N1R. For less energetic disruptions (which have more large fragments of similar mass), the largest fragments could form a moonlet belt, acting as both a source and a sink to ring particles, as in the case of the G ring of Saturn. Although our numerical model is not sufficiently advanced to differentiate between such specific outcomes, they are consistent with the character of the mass and velocity distributions produced by our simulations.

IV. ANALYTIC ESTIMATES OF STEADY-STATE POPULATIONS

In our numerical model we have considered only accretionary growth processes: erosion and fragmentation processes have been ignored. While coherent bodies will not undergo significant fragmentation for impact velocities considered in this work, some erosion of previously accumulated debris is likely to occur during nonaccreting collisions. The largest bodies in a swarm will therefore act as sources, as well as sinks, for smaller particles. The debris swarms studied here will eventually achieve a steady-state balance between the generation of ring particles through collisional erosion and the "sweep up" of ring particles as they accumulate onto the ringmoons. The ringmoons will experience mutual collisions but will not accrete with one another due to tidal restrictions in the Roche zone.

The properties of the steady state between particle accumulation onto the ringmoons and ejection of particles during nonaccreting collisions may be analytically estimated. The rate at which "particles" (i.e., those bodies which are described by the transient states of our Markov chain) are accreted onto "ringmoons" (i.e., those bodies which occupy absorbing states of our Markov chain, whose mass range is given by Eq. (35)) may be written

$$\frac{dN_{\text{f}}}{dt} = \frac{\alpha N_{\text{f}}}{T_{\text{c}}}, \tag{36}$$

where N_{f} is the number of free particles at time t, α is the accretion efficiency per collision, and $1/T_{\text{c}}$ is the rate at which a free particle collides with any ringmoon. The rate of production of free particles during nonaccreting collisions between the ringmoons is

$$\frac{dN_{\text{r}}}{dt} = \frac{\delta N_{\text{r}}}{T_{\text{r}}}, \tag{37}$$

where N_r is the number of particles which have accreted onto ringmoons at time t, δ is the fraction of a ringmoon's regolith which is ejected during a nonaccreting collision with another ringmoon, and $1/T_r$ is the rate at which a ringmoon collides with another ringmoon, so that T_r/δ is the lifetime of a particle in a ringmoon's regolith. At steady state the rate of production of particles will equal the rate of sweep-up of particles. Let X_f be the fraction of particles at time t which are in free orbits. Then at steady state,

$$\frac{\alpha X_f}{T_c} = \frac{\delta(1 - X_f)}{T_r} \tag{38}$$

or

$$X_{eq} = \left[1 + \frac{\alpha T_r}{\delta T_c}\right]^{-1}, \tag{39}$$

where X_{eq} is the fraction of unaccreted particles at steady state.

The collision rate between a high-velocity particle and the ringmoons (T_c) is accurately described by the PIAB collision frequency. A realistic collisional rate among the ringmoons (T_r), which are often few in number, requires more careful consideration. Velocity evolution in a swarm results in the largest bodies in the swarm occupying nearly circular and coplanar orbits (e.g., Wetherill and Stewart 1993). The largest bodies in the swarm will become physically isolated from one another if their radial separation exceeds their range of gravitational influence. Wetherill and Stewart (1993) account for noncrossing orbits of the largest bodies in their collision rate determination by assuming that bodies contained in mass bins for which $N_i R_g < W$ are isolated from one another. Here N_i is the number of bodies in mass bin i, W is the width of the swarm, and R_g is the gravitational range of a body, defined by

$$R_g(i) = \frac{2}{\sqrt{3}} R_{Hill}(i, i) + 2ae_i, \tag{40}$$

where e_i is the mean eccentricity in bin i. While this treatment still neglects the potential for resonances which could preclude collisions between moonlets with orbital separations less than R_g, it represents a better approximation than a straight PIAB approach. We note that the use of the PIAB collision frequency to model collisions among ringmoons in our numerical model does not significantly affect the results of our simulations, since ringmoon collisions do not result in accretion.

The accretion efficiency upon collision, α, is probably close to unity for collisions which satisfy our capture criteria. Numerical simulations by Ohtsuki (1993) show accretion probabilities greater than 80% for collisions with $r_p \lesssim 0.7$ and $\varepsilon = 0.5$. Collisions of small bodies into regolith-covered surfaces are likely to be much more inelastic than this, and as such will have even higher accretion probabilities. A value of $\alpha = 1$ is assumed for collisions which satisfy our two capture criteria.

A realistic value for δ is probably significantly smaller than unity. When two regolith-covered moonlets collide, the moonlet cores will likely bore through their partner's regolith layer until the cores impact. At low impact velocities the solid cores will not experience significant fragmentation or erosion, but as regolith is compacted and displaced at the impact site ejection of loose regolith material will occur. Ejection due to low-velocity impacts into regoliths has not been well-studied by previous impact experiments, which have focused on high-velocity impacts and catastrophic disruptions. However, some basic comparisons can be made. A low-velocity impact into regolith is most analogous to the so-called "gravity regime" of crater scaling, where the internal strength of the ejected material is ignored (e.g., Asphaug and Melosh 1993). If we consider a head-on collision between two like-sized ringmoons, the total volume of regolith which is displaced on one moon due to the collision is approximately given by

$$V_c \approx \left[\frac{2\pi}{3} R^3 \left(1 - \frac{R - d}{R}\right)\right], \tag{41}$$

where R is the radius of the ringmoons and d is the depth of the regolith. Some portion of this volume of ejecta will escape from the vicinity of the ringmoons, while the rest will reimpact. In the gravity regime, the fractional volume of ejecta exceeding escape velocity can be expressed as

$$\frac{V_{esc}}{R_c} = k_3 \left(\frac{v_{esc}}{\sqrt{gR_c}}\right)^{-e_v}, \tag{42}$$

where R_c is the radius of the "crater" formed in the regolith, v_{esc} is the escape velocity, g is the gravity field, and k_3 and e_v are experimentally determined constants (Asphaug and Melosh 1993). Equation (42) predicts a maximum fraction of ejecta escaping of about 0.2 for values of k_3 and e_v corresponding to impacts into sand or rock, assuming a crater diameter equal to the target radius (see Asphaug and Melosh 1993, their Fig. A1).

In the Roche zone, the true escape velocity from the surface of a moon can be less than the two-body escape velocity, depending on ejection orientation. Monte Carlo simulations of ejecta produced by impacts into Phobos (located inside the classical Roche limit) which account for the tidal effects of Mars show appreciable escape probabilities for velocities as low as $\sim 0.35 v_{esc}$ (Banaszkiewicz

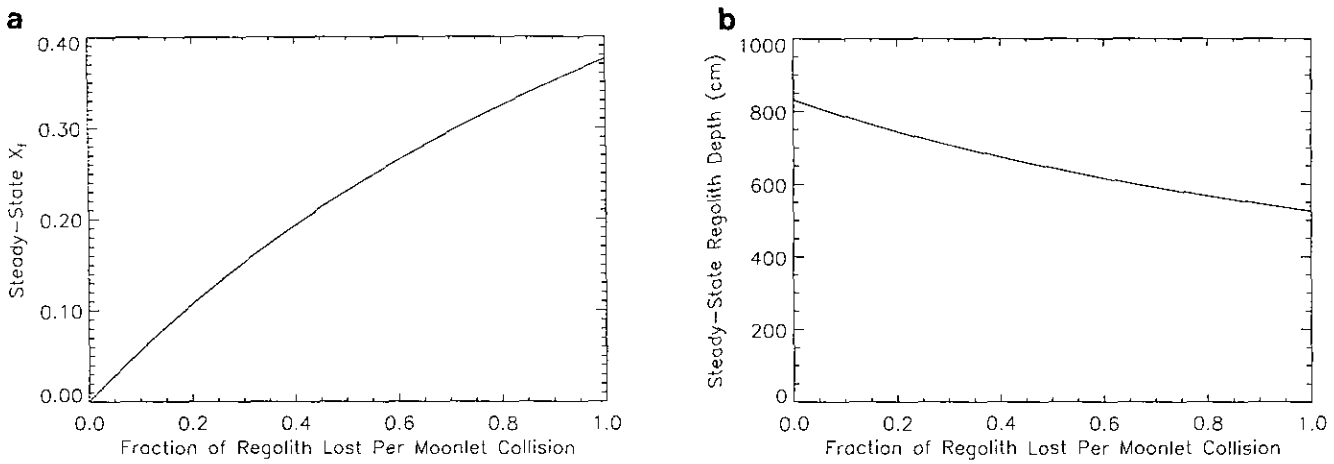

FIG. 8. (a) The steady-state fraction of unaccreted material as a function of the fraction of regolith which escapes during a collision between two ringmoons (δ) for the simulation shown in Fig. 5a. An estimate for δ derived from basic ejecta scaling arguments yields $\delta \sim 0.12$. (b) The corresponding steady-state average regolith depth on a ringmoon.

and Ip 1991). Using this value as an estimate for average escape velocities near the Roche limit yields the upper limit on the fraction of ejecta escaping to be about 0.74 of the total ejected volume. The fraction of the total regolith on a ringmoon which is ejected upon mutual collision is therefore estimated to be

$$\delta \sim 0.74 \frac{V_c}{4\pi R^2 d} \sim 0.12, \tag{43}$$

which is independent of R and d assuming a uniform regolith depth on a ringmoon.

For the simulation shown in Fig. 5a, the Wetherill and Stewart (1993) collision criterion yields the time for a ringmoon to collide with another ringmoon (T_r) to be about 1100 years. The time scale for a particle to collide with a ringmoon (T_c) is about 650 years. Figure 8a shows that in this case, X_{eq} varies between 0 and 0.38 for δ between 0 and 1, with $\delta = 0.12$ corresponding to $X_{eq} = 0.06$. Figure 8b shows the average regolith depth on a ringmoon at steady state, with $\delta = 0.12$ corresponding to a depth of about 8 m. For comparison, after 600 years the remaining fraction of free particles in the mass distribution shown in Fig. 5a is about 0.08. It thus seems unlikely that the debris swarm at the Adams ring would evolve significantly beyond the final mass distribution shown in Fig. 5a, due to competing erosional processes, and our results approximate the steady-state distribution.

The debris swarm evolution shown in Fig. 7 is more difficult to interpret using our basic analytic approach. In considering a balance between the rate of accretion of particles onto the ringmoons and the rate of erosion of particles from the ringmoons we have made the simplifying assumption that particles collide more frequently with ringmoons than with other bodies found in the "transient" mass states. This is a valid assumption for distributions which have most of their mass contained in the largest bodies, as in Fig. 5. However, in Fig. 7 we consider a mass distribution whose high-mass end is steeper than the equal mass per bin case, so that particles accrete most rapidly onto bodies smaller than the smallest absorbing state. In this case, although only bodies with mass greater than about 10^{13} g are prohibited from accreting onto larger bodies by tidal forces, accretion of bodies in the mass range of 10^{10}–10^{12} g onto larger bodies is extremly slow, and these intermediate bodies accumulate appreciable regoliths before finally accreting onto the ringmoons. Determination of steady-state populations in this case requires an incorporation of erosion production on a collision by collision basis, which is beyond the scope of this work.

As a final comment on potential effects of erosional processes, we note that our analytic approach has neglected any dependence of escape on regolith particle size. Small regolith particles may be ejected with relatively higher ejection velocities (e.g., Nakamura and Fujiwara 1991) and thus may escape more easily and steepen the steady-state distribution in the small mass end from that produced by our simulations. Meteoroid impacts into the ringmoons will also eject regolith. Time scales for impact of a 10^3-g meteoroid onto a ringmoon are about 10^5–10^6 years–much longer than time scales for collisions between ringmoons (Colwell and Esposito 1990). Although ejection of regolith due to meteoroid impacts will not be significant for the size range of particles considered here, production rates of micrometer-sized dust particles due to meteoroid impacts can be on the order of dust production rates due to collisions between the ringmoons

(Colwell and Esposito 1990). This would also lead to a steepening of the mass distribution for dust-sized particles relative to that produced in our simulations. Conversely, large particles in the regolith lie closer to the edge of their Hill sphere and so, depending on their ejection orientation, will typically have lower effective escape velocities than their smaller counterparts. Some replenishment of the intermediate mass region between the ring particles and the ring moons relative to that shown in Fig. 7 particularly might therefore be expected.

V. COMPARISONS WITH PAST WORKS

A. Comparisons with Previous Accretion Models

1. Weidenschilling et al. (1984). In the "DEB" (dynamical ephemeral bodies) numerical model, Weidenschilling *et al.* (1984) used a two-body criterion for accretion and allowed for tidal disruption of particles when tidal stresses exceeded estimates of internal tensile strength. The latter condition defines a maximum particle radius which may exist at a given orbital location as a function of internal strength. In their numerical simulations, Weidenschilling *et al.* (1984) did not account for self-gravity in their tidal disruption criteria. This is a valid assumption for solid, coherent bodies smaller than about 20 km in radius that have internal strengths much greater than their self-gravity. However, aggregate bodies formed through the accumulation process have initially very low (if any) internal strengths and are likely initially held together due to self-gravity (Salo 1992, Longaretti 1989).

Our method differs from the Weidenschilling *et al.* model in two ways. First, we use three-body capture criteria as described in Section II.C. Second, we do not consider the internal strength of accreting bodies; we instead balance self-gravity against tidal stress. In the DEB model, the balance of internal strength and tidal stress results in tidal stresses which increase with size; in contrast, the balance of self-gravity and tidal stress is independent of size for a given particle density. In the Hill formalism this is expressed by the fact that the ratio of a body's physical radius to its Hill sphere is a function of density, not of size. We therefore do not place a restriction on the absolute size which a body of a given density can grow to at a given orbital location; the growth of bodies is limited only by our capture criteria.

Our results differ from the DEB model in several fundamental respects. First, Weidenschilling *et al.* find that accretion is the dominant result of low-velocity, inelastic collisions in Saturn's rings. This is certainly the case when a two-body criterion for capture is used. However, we find that this conclusion is changed significantly when the capture criteria includes the effects of the tidal potential. Our results show that accretion in most rings occurs only between bodies who differ greatly in mass and that buildup of large objects through the accumulation of many smaller "building blocks" is therefore an ineffective process. Neither this work nor that of Salo (1992) finds gravitational-based accretion between bodies with a density of solid ice in Saturn's D, C, and B rings. We cannot rule out the possibility of physical mechanisms leading to limited sticking in these regions.

Weidenschilling *et al.* proposed that the largest bodies in rings represent either cohesive fragments or house-sized aggregate bodies in equilibrium between accretion and tidal disruption (the DEBs). This work supports the conclusion that the largest bodies in a ring likely represent cohesive fragments from earlier disruption events. These cohesive cores may accumulate smaller bodies, but they do not grow significantly in size. While their surfaces are likely to be "dynamic," as smaller bodies accrete and are knocked off by later collisions, cohesive ice cores are stable against tidal disruption due to their self-gravity in all regions of Saturn's rings.

Weidenschilling *et al.* also suggest that ring particles are in an ensemble steady state between accretion of bodies up to a limiting size and tidal disruption. We propose a potential steady state between accretion of small bodies onto large bodies and production of small bodies through external bombardment and mutual collisions, with tidal forces dictating the character of accretion which can occur and the minimum density of gravitationally bound aggregates. The overall character of such a system would evolve on time scales determined by the collisional lifetimes of the large bodies, that, once disrupted, would be unable to reaccrete.

2. Longaretti (1989). In his analytical study of the effects of various physical processes on the size distribution of particles in Saturn's main ring, Longaretti (1989) accounted for tidal effects on accretion using a force approach. Longaretti considered the case of two radially aligned particles initially in contact with no relative velocity and examined when the pair would experience a net attractive gravitational force in a tidal environment. This condition defines both a maximum size ratio and a minimum particle density for accretion as a function of orbital location (his Eq. (29)). In our notation, Longaretti's Eq. (29) yields a $r_p < 1$ criterion for accretion. This is a less severe restriction than our $r_p \lesssim 0.691$ criterion. Similarly, the critical density for accretion given in our Eq. (32b) is larger by about a factor of 3 than the critical density found by Longaretti (his Eq. (30)). The differences in accretion criteria between the two works is a result of our adopting an energy-based approach, where both relative initial kinetic and potential energies are considered, and our assumption that particles collide with random orientation.

From his three-body capture criterion, Longaretti concluded that aggregates appear to be a natural outcome of ring particle collisions, and that the fractional mass gain during a collision can be of order unity. Our results support this conclusion only for the very outer ring systems (see Table I). Longaretti also investigated the coupling of translational and rotational degrees of freedom during collisions; these results, relevant to determination of more accurate coefficients of restitution than we have modeled here, are discussed in Section VI.

3. Salo (1992). Salo (1992) conducted numerical N-body simulations of ring particle interactions, including both gravitational interactions and dissipative collisions. His simulations show that gravitational wakes which form in Saturn's outer rings are in some cases strong enough that trapped particles can form gravitationally bound, low-density aggregates. Sale finds that for an initial distribution of particles with a density of solid ice (0.9 g/cm^3), spanning an order of magnitude in radius (50 cm $< r <$ 5 m), aggregate bodies begin to form between 2.07 and 2.16R_S in Saturn's A ring. He does not find any accretion in Saturn's C ring or B ring. At 2.12R_S, Salo finds an aggregate body which grows to a radius of 15 m, with a density of 0.3 g/cm^3, at which point its accretional growth stops.

Qualitatively, our estimates for accretional growth match Salo's numerical results well. Our model predicts that gravitational accretion will not occur in Saturn's C ring and B ring and that accretion at the inner edge of the A ring (2.02R_S) will occur only for small mass ratios (from Table I), consistent with Salo's results.

Specifically, our model predicts that accretion at 2.12R_S should occur to a lesser extent than seen in Salo's simulations. With a particle density of 0.9 g/cm^3 at 2.12R_S, our accretion model permits accretion only between bodies whose mass ratio is less than 0.0013; Salo's simulations show aggregate formation between bodies whose mass ratio is higher than this. We can directly compare Eq. (31) to Salo's finding that a 15-m object whose density is 0.3 g/cm^3 can no longer accumulate 50-cm particles. The combination of the underdense 15-m aggregate and a 50-cm particle of density 0.9 g/cm^3 would have a combined scaled size of $r_p \approx 0.89$ in Hill units. That this combination does not result in accretion implies a $r_p \lesssim 0.89$ criterion for accretion, a less stringent criterion than our Eq. (31).

There are several possible explanations for the specific differences between our model's results and those of Salo. While Salo's N-body simulations allow for decreasing densities as aggregates form with void spaces, our model assumes a constant density for all bodies. Salo's aggregate particles can also deform during collisions, so that the physical scaled radius of a composite particle can be smaller than the value of r_p given by Eq. (21) and thus can fill a smaller portion of its Hill sphere than we would predict. This is particularly true when the composite body is much larger than all of its constituent parts. Nonetheless, by assuming constant densities appropriate for solid ice/rock bodies, our model will still tend to overestimate accretion, since accretion between strength-dominated ($r \lesssim 20$ km) bodies will in general produce aggregate bodies with densities less than that of solid bodies. Our neglect of the physical shapes and evolving densities of individual bodies thus does not account for the greater extent of accretion found by Salo.

We instead believe that the discrepancies between Salo's findings and our predictions are mainly a result of our model's treatment of each collision as a three-body problem; gravitational interactions of orbiting particles not involved in a collision are ignored in our capture criteria. The formation of gravitational wakes in dense rings is a collective phenomena which will alter the gravitational potential felt by colliding bodies from that of the simple three-body case, as the influence of nearby bodies helps to offset the tidal influence of the planet. In the case of the outer A ring, gravitational instabilities seem to foster the buildup of low-density aggregates. Additionally, by adopting a capture criterion based on average impact orientations we have neglected some collisions which may result in accretion for certain impact directions. In dense rings, where particles experience both a large number of impacts per orbit and collective gravitational effects such as wake formation, the effects of impact orientation may be significant. Collective effects are unlikely to be important in low-optical-depth rings and moonlet belts.

B. Implications for Specific Questions of Ring and Moon Origins

1. Lifetimes of small moons. Colwell and Esposito (1992, hereafter CE92) calculated lifetimes for the small moons of Uranus and Neptune listed in Table I as short as 80 million years (for Cordelia). Assuming that the observed moon population represents collisional fragments, CE92 found that the evolution of the collisional cascade requires both large satellites to act as initial parent bodies (a 100-km-radius body is needed to act as a primordial source for Cordelia and Ophelia) and that surprisingly large numbers of 1- to 10-km bodies currently coexist with the observed small moons (about 1000 1 km radius bodies at the ϵ ring). Although both of these somewhat difficult conclusions could be tempered by the inclusion of accretionary processes, this work indicates that for reasonable particle density estimates, accretion is not possible at the current orbital locations of Cordelia, Ophelia, Naiad, Thalassa, and Despina. Low mass ratio accretion is possible for the other moons; for example, at its current orbital position, Bianca could accrete a 3-km-radius body with

a low relative impact velocity. However, such loosely bound "rubble-piles" would surely have lower internal strengths than those considered by CE92, and would therefore have shorter lifetimes against disruption than their solid counterparts. A combination of the assumption of a constant impactor flux with time and the neglect of orbital tidal evolution of moons may have led CE92 to underestimate moon lifetimes. However, since CE92 found the smallest moons to have lifetimes less than about 250 million years, their estimates would have to be in error by more than a factor of 10 to produce moon lifetimes dating back to the era of planet formation. This seems unlikely. In short, reaccretion alone cannot end the quandary over the existence of the current populations of small, and thus short-lifetime moons observed by Voyager. In fact, when Cordelia, Ophelia, Naiad, Thalassa, or Despina are eventually disrupted by a meteroid or cometary impact, their fragments will not reaccumulate. These moons are today's ring precursors.

2. *Neptune's inner satellites.* Banfield and Murray (1992) require that the current inner satellite system at Neptune accreted after the circularization of Triton's orbit. Their Fig. 2 models the tidal history of the current satellites over the past 4 billion years, using a maximun rate of tidal evolution based on Larissa's formation at corotation. Our work indicates that Naiad and Thalassa could not have formed through accretion, even at their estimated initial semimajor axes of $2.02R_N$ and $2.2R_N$. This work supports the Banfield and Murray suggestion that these two moons may represent fragments from the disruption of a larger object which formed at a more distant orbital location and experienced greater tidal orbital evolution due to its greater mass. It appears very unlikely that the rest of the debris produced from such a disruption gravitationally accumulated onto Naiad or Thalassa; perhaps some of it is currently resides in the ring arcs. Limited accretion is possible at the estimated initial positions of Larissa, Galatea, and Despina, although the latter case is very difficult for densities less than 1.4 g/cm^3.

3. *G-Ring parent bodies.* In a recent analysis of photometry of the G ring, Showalter and Cuzzi (1993) have inferred the presence of a band of parent bodies, ranging in size from 100 m to 1 km. It has been difficult to explain how such bodies would not reaccrete, since the G ring is located well outside the classical Roche limit. We find that if the parent bodies have a density of solid ice, they could not accrete in the G ring unless their radii differed by more than about 50% and then only if rebound velocities are very low. Accretion of like-sized objects could occur only for densities $\geq$1.5 g/cm^3, which seems high given that the known densities of Saturn's inner moons are in the 1.17–1.26 g/cm^3 range. It is plausible that a small population of parent bodies in a relatively narrow size range could coexist in the G ring without accumulating, acting as a source and sink for the dusty ring material.

VI. CONCLUSIONS AND FUTURE WORK

The results presented here demonstrate the intriguing and unusual character of accretionary processes in a tidal environment. Additionally, they suggest that tidally modified accretion may play a significant part in the origin and evolution of coexisting ring/ringmoon systems. Our main conclusions follow.

1. *The type of accretion which occurs in the Roche zone has a very different character than simple hierarchical accretion. Small bodies accrete onto large bodies, while like-sized objects are prevented from accreting with one another due to the tidal influence of the planet.* Table I lists the maximum mass ratio between colliding bodies which can result in accretion at various ring and satellite locations. Accretion between bodies who differ greatly in mass is possible within the classical Roche limit, while bodies close in mass are precluded from accreting in regions exterior to the Roche limit.

2. *Accretional growth of ice–rock bodies* ($0.9 \lesssim \rho \lesssim 1.5$ *g/cm*^{3}) *is extremely limited by tidal influences within all ring systems.* We find very limited accretional growth, despite the fact that the major approximations inherent to our formalism will lead to an overestimation of accretion. These include the neglect of erosion and fragmentation, the assumption of constant density, and the use of a fixed-bin mass state vector.

3. *"Runaway accretion" or complete reaccumulation of disrupted bodies is not found to occur in the Roche zone.* We find that for $a \lesssim (\rho/\rho_p)^{-1/3}3R_p$, where ρ is the density of the accreting material and ρ_p and R_p are the density and the radius of the planet, tidal effects on accretion drastically reduce or eliminate significant growth of the largest bodies in a swarm. As a consequence, we conclude that cohesive ice or rock bodies can stably exist at orbital radii far interior to regions where such bodies can efficiently accumulate from debris distributions.

4. *Tidally modified accretion can lead to the formation of bimodal populations, with one element composed of many small, high-velocity particles and the other of a few large objects on nearly circular orbits. Ring/ringmoon systems may be the natural result of accretional evolution of a fragmentation-produced debris distribution in the Roche zone.* This is the first work to offer a quantitative explanation for the origin of the bimodal character of ring/ringmoon systems, as well as an explanation for the stable coexistence of large objects outside the classical Roche limit.

With a combination of relatively direct numerical and analytic approaches we have been able to draw several

interesting conclusions about accretion in the Roche zone. Our preliminary model has included several significant assumptions and approximations. The Markov accretion model described here assumes a constant density for all bodies, independent of their individual histories. In reality, the density of agglomerate bodies will typically be lower than that of their constituent bodies due to void spaces, since the self-gravity of bodies less than about 20 km in radius is typically not strong enough to overcome the internal strengths of the composite particles. For accretion between like-sized bodies, large void spaces will quickly result in underdense ($\rho \sim 0.1$ g/cm^3) DEBs as proposed by Weidenschilling *et al.* (1984). Because accretion in a tidal environment occurs preferentially between bodies which differ greatly in size, density should not decrease as much during the course of accretion, since smaller bodies are better able to fill in void spaces. However, some decrease in density will still occur as objects accrete in the Roche zone. Altenatively, underdense aggregates may experience an increase in density as they deform while accreting smaller bodies. In general, the neglect of density evolution by this work results in an overestimation of the amount of accretion which can occur, since lower density objects are more likely to overflow their Hill sphere. When agglomerates of very low density form in most rings, through physical sticking mechanisms, spatially asymetric accretion, or accretion of bodies close in size (for outer rings), they would be only marginally (if at all) gravitationally bound, and would likely be dispersed during future impacts. Some underdense agglomerates may form in dense rings due to collective gravitational effects (Salo 1992), as discussed in Section V.A.3.

This model considers only gravitation-based accretion. Physical sticking processes, caused by interparticle surface forces, could be significant for small particles with high surface-area-to-mass ratios. While physical or chemical bonds formed between micrometer-sized bodies may lead to the formation of dust aggregates, recent experiments do not find sticking between such aggregates, even at low velocities (Blum and Münch 1993). The overall effect of sticking processes on macroscopic accretion would seem to be small.

The capture criteria dervied in this work are based on the assumption of random impact orientation. The specific extent of the mass range left relatively unaffected by accretion (Eq. (35)) is dependent on the critical value of r_p needed for accretion, which we have derived using an angle-averaged impact energy. Consideration of specific impact orientations changes this critical r_p value, which in turn affects the number of mass "states" contained in the high-mass end of the bimodal distributions shown in Figs. 5a and 7. If the critical r_p for accretion on average is higher than the angle-averaged value (which could be the case if most impacts occur radially), the high-mass end will cover a smaller mass range at a given orbital radius. Figure 9 shows the evolution of the swarm from Fig. 5a with a critical value of $r_p = 0.75$. For the case of accretion at the Adams ring, the bimodality is preserved for critical values of r_p less than about 0.93; this value would instead lead to the bimodality seen in Figs. 5a and 7 at more interior orbital locations. An average critical value of r_p needed for accretion which is close to unity would imply that nearly all collisions occur radially and that bodies in the swarm do not "spin" significantly (since this would tend to rotate a previously radially accreted particle into a narrower dimension of the Hill sphere, where it would be easily ejected upon subsequent impacts). A higher average critical value for r_p may also be appropriate for high optical depth rings ($\tau \gtrsim 0.2$) where collective gravitational effects are significant (Salo 1994).

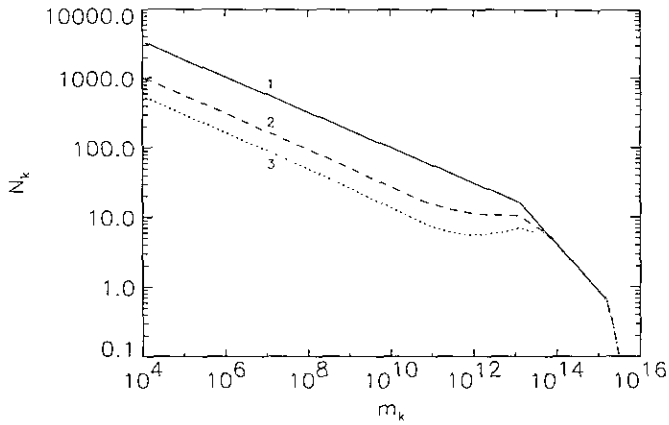

FIG. 9 The mass evolution of a debris swarm at the Adams ring. Same conditions as Fig. 5a, except here the critical value of r_p required for accretion has been raised to $r_p = 0.75$, which has decreased the number of "absorbing states" by one. Mass distributions 1–3 are shown for $t = 0$, 300, and 450 years.

The collision rate formalism utilized here is appropriate only for swarms consisting of a large number of bodies with high random velocities. As velocities are collisionally damped and accretion progresses, the PIAB approximation fails. In order to study accretion at relative velocities lower than those discussed here, we will need to utilize collision frequencies appropriate to low-velocity, shear-dominated collisions. Expressions for the low-velocity regime have been derived for the domain of planetary accretion (see, e.g., Greenberg *et al.* 1991); however, expressions valid in a highly tidal environment are still required.

The coefficient of restitution of a collision is crucial in determining whether colliding bodies will eventually become gravitationally bound. In our model, ε is treated as a constant parameter. The extreme case of completely inelastic collisions (Figs. 5 and 7) demonstrates the great-

est extent of gravitational accretion possible, while the case of completely elastic collisions results in no accretion for all of the ring and satellite systems discussed here. In reality, the coefficient of restitution is a function of both impact velocity and of particle size. Experimental results of Hatzes *et al.* (1988) indicate that ε tends to decrease with increasing velocity. Analytic modeling by Dilley (1993) and Blum and Münch (1993) suggests that for a given particle size, a collision with a like-sized body will be more inelastic than one with a much larger body. However, the absolute size of the smaller body seems to play an important role, as all mass-ratio collisions appear to be more elastic as the size of the smaller body increases (see Dilley 1993, Fig. 5). These trends all seem to decrease the likelihood for accretion between large, low-velocity objects, although more exact functional dependences of ε on velocity, size, and mass are needed to determine the specific implications for accretion processes.

Determining exact amounts of energy damping during collisions of orbiting bodies is yet still more complex. While experimental work has focused on the determination of normal coefficients of restitution, ε_n, theoretical modeling by Longaretti (1989) has examined both translational and rotational degrees of freedom during collisions. His work indicates that coupling between these degrees of freedom can result in rebound velocities which are greater than zero even when coefficients of restitution are equal to zero. If the effective coefficient of restitution as defined in Eq. (27) is greater than about 0.5, due to either elastic physical properties of rock/ice fragments or to particle spin following collisions, the onset of accretion between particles with $\mu < \mu_{crit}$ will not begin until velocities have been significantly collisionally damped. In this work, we have adopted a collision frequency scheme valid when impact velocities are determined predominately by random velocities. However, for very elastic collisions accretion will occur as impact velocities are increasingly determined by Keplerian shear, and collision rates valid for shear-dominated collisions will be required. This is demonstrated by the values of ε_{crit} listed in Table I, which represent the maximum values of ε which can, on average, result in accretion between objects in the PIAB regime. As mentioned above, expressions for shear-regime rates currently available are invalid in the Roche zone. One of the important future directions of this work will be the development of such rates and an analysis of accretion processes near the Roche zone at low relative velocities. This will be crucial in the modeling of both the final stages of accretion in tidal environments, when velocities of the largest bodies have been significantly damped due to collisional damping, and to modeling accretion in swarms where the effective coefficient of restitution during collisions is higher than the ε_{crit} values given in Table I.

Our preliminary model has demonstrated that the effects of tidal forces can significantly alter the course of accretion in the Roche zone. Even as collisional velocities are damped due to inelastic collisions, bodies with similar masses cannot accrete with each other in the Roche zone due to the influence of the tidal potential. In certain cases, our simulations show that this leads to a bimodal population, with one component consisting of smaller, meter-sized objects and the other of a few tens of bodies of hundreds of meters to kilometers in size. These large bodies continue to sweep up small bodies and dust, but are precluded from accreting with each other by the tidal potential. This bimodality is suggestive of one of the most striking features of the Voyager results: the common coexistence of dust, rings, and ringmoons around the giant planets.

APPENDIX A

Derivation of Mass Transition Probabilities

The time rate of change of the total amount of mass contained in the kth mass bin, M_k, is given by

$$\frac{dM_k}{dt} = (A + B + C) - (D + E + F). \tag{A1}$$

where A, B, and C are integrals which represent mass gain to the kth bin and D, E, and F are integrals which represent mass loss from the kth bin. The gain integrals are

$$A = \int_{m_{k-1}}^{m_k} dm'' \int_{m_{k-1}}^{m_k} dm' \frac{1}{2}(m' + m'')n_{m'}n_{m''}A_{m',m''} \tag{A2}$$

$$B = \sum B_j = \sum_{j=1}^{k-2} \int_{m_j}^{m_{j+1}} dm'' \int_{m_k - m''}^{m_k} dm'(m' + m'')n_{m'}n_{m''}A_{m',m''} \tag{A3}$$

$$C = \sum C_j = \sum_{j=1}^{k-1} \int_{m_j}^{m_{j+1}} dm'' \int_{m_k}^{m_{k+1} - m''} dm'(m'')n_{m'}n_{m''}A_{m',m''}, \tag{A4}$$

where A represents mass gain to the kth bin due to collisions between particles in the $(k-1)$th bin, B represents gain due to collisions between the $(k-1)$th bin and all smaller bins, and C represents mass gain to the kth bin due to collisions between kth bin particles and all smaller bin particles. The amount of mass transferred to the kth bin as a result of a particular collision is in parentheses in each integral, $n_m dm$ is the differential mass distribution within a bin, and $A_{m',m''}$ is the accretion probability per time.

The loss integrals are given by

$$D = \int_{m_k}^{m_{k+1}} dm'' \int_{m_k}^{m_{k+1}} dm' \frac{1}{2}(m' + m'')n_{m'}n_{m''}A_{m',m''} \tag{A5}$$

$$E = \sum E_j = \sum_{j=k+1}^{Y-1} \int_{m_j}^{m_{j+1}} dm'' \int_{m_k}^{m_{k+1}} dm'(m')n_{m'}n_{m''}A_{m',m''} \tag{A6}$$

$$F = \sum F_j = \sum_{j=1}^{k-1} \int_{m_j}^{m_{j+1}} dm'', \int_{m_{k+1} - m''}^{m_{k+1}} dm'(m')n_{m'}n_{m''}A_{m',m''}, \tag{A7}$$

where Y is the total number of mass bins. Integrals D, E, and F describe the loss of kth bin particles as they accrete with other particles to produce larger objects. Integral D represents mass loss from the kth bin due to

collisions between kth bin particles, E represents loss due to collisions between kth bin particles and all larger bin particles, and F represents mass loss from the kth bin due to collisions between kth bin particles and all smaller bins. Integrals (A2)–(A7) account for all possible sources of mass gain to or mass loss from the kth bin in a purely accreting system; these integrals apply only to mass bins spaced logarithmically by a factor of 2 in mass.

The transition matrix element $T(i, k)$ is the probability that a unit mass will be transferred from bin i to bin k in time Δt. A little algebraic manipulation is needed to derive the matrix elements from Eqs. (A2)–(A7). Integrals A and C describe mass transfer rates to the kth bin from a single smaller bin (the $(k-1)$th bin or the jth bin), while integrals D, E, and F all describe rates of mass transfer from mass bin k to a single larger mass bin (the $(k+1)$th bin for D and F and the jth bin for E). However, integral B describes the rate of mass transfer from two mass bins—the $(k-1)$th and the jth bins—to the kth bin. For this reason, integral B is divided into two parts when defining the transition matrix elements:

$$B = B_1 + B_2 \tag{A8}$$

$$B_1 = \sum B_{1,j} = \sum_{j=1}^{k-2} \int_{m_j}^{m_{j+1}} dm'' \int_{m_k - m''}^{m_k} dm'(m'') n_{m'} n_{m''} A_{m',m''} \tag{A9}$$

$$B_2 = \sum B_{2,j} = \sum_{j=1}^{k-2} \int_{m_j}^{m_{j+1}} dm'' \int_{m_k - m''}^{m_k} dm'(m') n_{m'} n_{m''} A_{m',m''}. \tag{A10}$$

Both mass transfers are the result of particles in the jth and $(k-1)$th bins accreting together to form new particles large enough to enter the kth mass bin. Here, B_1 is the rate of mass transfer to the kth bin from bin j, and B_2 is the rate of mass transfer to the kth bin from the $(k-1)$th bin.

The transition matrix elements are therefore given by

$$T(i,k) = \begin{cases} [B_{1,i} + C_i] \cdot \Delta t & \text{if } i < (k-1) \\ [A + B_2 + C_{k-1}] \cdot \Delta t & \text{if } i = (k-1) \\ 1 - [\{D + E + F\} \cdot \Delta t] & \text{if } i = k \\ 0 & \text{if } i > k \end{cases}, \tag{A11}$$

where A thru F are given by Eqs. (A2)–(A10), i and k range from 1 to $(Y-1)$, and Δt is the size of the time step.

The transition matrix elements which describe mass transfer to the final, discrete bin are given by

$$T(i,Y) = \begin{cases} [B_{1,i}] \cdot \Delta t & \text{if } i < (Y-1) \\ [A + B_2 \cdot \Delta t] & \text{if } i = (Y-1). \\ 1 & \text{if } i = Y \end{cases} \tag{A12}$$

Since $T(Y, Y) = 1$, the final bin is an *absorbing state*. Note that the integrals present in Eq. (A13) do not involve collisions with the final Yth bin. This is because in a real system the final bin as defined in our model is occupied only when all other bins are empty.

APPENDIX B

Velocity Evolution Due to Accretion

The evolution of the rms velocity of each mass bin is affected by two basic processes: distant, gravitational interactions between bodies and inelastic collisions. We have utilized the work of Stewart and Wetherill (1988) to model how the rms velocities of each mass bin evolve due to gravitational stirring, inelastic rebounding collisions, and dynamical friction with all other bins. Below we derive an analogous expression for the rms velocity evolution due to accretion.

Consider the total change in kinetic energy the kth mass bin experiences per unit time,

$$\frac{d(M_k \langle v^2 \rangle)}{dt} = M_k \frac{d\langle v^2 \rangle}{dt} + \langle v^2 \rangle \frac{dM_k}{dt}, \tag{B1}$$

where M_k is the total amount of mass in the bin and $\langle v^2 \rangle$ is the mean square random velocity of the bin. Ignoring mass evolution, $dM_k/dt = 0$, and we have

$$\frac{d(M_k \langle v^2 \rangle)}{dt} = M_k \left[\left. \frac{d\langle v^2 \rangle}{dt} \right|_{\text{stir}} + \left. \frac{d\langle v^2 \rangle}{dt} \right|_{\text{reb}} + \left. \frac{d\langle v^2 \rangle}{dt} \right|_{\text{fric}} \right], \tag{B2}$$

where the terms on the right-hand side correspond respectively to velocity evolution due to gravitation stirring, inelastic rebounding, and dynamical friction as given by Stewart and Wetherill (1988).

The change in kinetic energy a mass bin experiences due only to accretion is given by the kinetic energy of mass entering the bin minus the kinetic energy of mass leaving the bin:

$$\frac{d(M_k \langle v^2 \rangle)}{dt} = \frac{1}{dt} \left[\sum_{i=0,k-1} M_i T(i,k) \langle v_{\text{cm}}^2 \rangle - M_k (1 - T(k,k)) \langle v^2 \rangle \right], \tag{B3}$$

where $T(i, k)$ and $T(k, k)$ are mass transition probabilities defined in Appendix A, $\langle v_{\text{cm}}^2 \rangle$ is the mean square velocity of the mass entering the bin (given by the center of mass velocity of the accreting pair) and we have assumed that mass leaving the kth bin has a square velocity given by the mean value for the bin, $\langle v^2 \rangle$. The total change in kinetic energy due to accretion can also be written in differential form:

$$\left. \frac{d(M_k \langle v^2 \rangle)}{dt} \right|_{\text{acc}} = M_k \left. \frac{d\langle v^2 \rangle}{dt} \right|_{\text{acc}} + \langle v^2 \rangle \left. \frac{dM_k}{dt} \right|_{\text{acc}}. \tag{B4}$$

Equating Eqs. (B3) and (B4) and solving for $(d\langle v^2 \rangle)/(dt)|_{\text{acc}}$ we find:

$$\left. \frac{d\langle v^2 \rangle}{dt} \right|_{\text{acc}} = \frac{\sum_{i=0,k-1} M_i T(i,k) \langle v_{\text{cm}}^2 \rangle - \langle v^2 \rangle \sum_{i=0,k-1} M_i T(i,k)}{dt \times M_k}. \tag{B5}$$

Equation (B5) is of the same form as the Stewart and Wetherill (1988) equations. It is comparable to Ohtsuki's (1992) Eq. (2.11), except here we have eliminated a term by assuming that mass which leaves a bin has a square velocity given by the mean value for the bin.

ACKNOWLEDGMENTS

This research was supported by the Cassini Project and the Patricia Roberts Harris Fellowship program. We acknowledge Glen Stewart for his many contributions to this work and for a thorough review of an earlier version of this paper and Joshua Colwell, Mihaly Horanyi and Richard Mihran for many fruitful discussions. We thank Heikki Salo and Pierrve-Yves Longaretti for their suggestions and thoughtful reviews of the manuscript.

REFERENCES

ARAKI, S., AND S. TREMAINE 1986. The dynamics of dense particle disks. *Icarus* **65**, 83–109.

ASPHAUG, E., AND H. J. MELOSH 1993. The stickney impact of phobos: A dynamical model. *Icarus* **101,** 144–164.

BANASZKIEWICZ, M., AND W.-H. IP 1991. A statistical study of impact ejecta distribution around Phobos and Deimos. *Icarus* **90,** 237–253.

BANFIELD, D., AND N. MURRAY 1992. A dynamical history of the inner neptunian satellites. *Icarus* **99,** 390–401.

BLUM, JÜRGEN, AND MICHAEL MÜNCH 1993. Experimental investigations on aggregate–aggregate collisions in the early solar nebula. *Icarus* **106,** 151–167.

CANUP, R. M., J. E. COLWELL, AND M. HORANYI 1993. Size distributions of satellite dust ejecta: Effects of radiation pressure and planetary oblateness. *Icarus* **105,** 363–369.

CANUP, R. M., AND L. W. ESPOSITO 1992. The re-accretion of disrupted planetary satellites. *Bull. Am. Astron. Soc.* **24,** 937.

COLWELL, J. E., AND L. W. ESPOSITO 1990. A numerical model of the uranian dust rings. *Icarus* **86,** 530–560.

COLWELL, J. E., AND L. W. ESPOSITO 1992. Origins of the rings of Uranus and Neptune: I. Statistics of satellite disruptions. *J. Geophys. Res.* **97,** 10,227–10,241.

COLWELL, J. E., AND L. W. ESPOSITO 1993. Origins of the rings of Uranus and Neptune: II. Initial conditions and ring moon populations *J. Geophys. Res.* **98,** 7387–7401.

DAVIS, D. R., AND E. V. RYAN 1990. On collisional disruption: Experimental results and scaling laws. *Icarus* **83,** 156–182.

DILLEY, J. P. 1993. Energy loss in collisions of icy spheres: Loss mechanism and size-mass dependence. *Icarus* **105,** 225–234.

DONES, L. 1991. A recent cometary origin for Saturn's rings? *Icarus* **92,** 194–203.

ESPOSITO, L. W. 1993. Understanding planetary rings. *Annu. Rev. Earth Plan. Sci.* **21,** 487–523.

ESPOSITO, L. W., AND R. M. CANUP 1993. Equivalence class structure of absorbing Markov chains: Application to accretion in the Roche Zone. *Bull. Am. Astron. Soc.* **25,** 1102.

ESPOSITO, L. W., AND L. L. HOUSE 1978. Radiative transfer calculated from a Markov chain formalism. *Astrophys. J.* **219,** 1058–1067.

GREENBERG, R., J. F. WACKER, W. K. HARTMANN, AND C. R. CHAPMAN 1978. Planetesimals to planets: Numerical simulation of collisional evolution. *Icarus* **35,** 1–26.

GREENBERG, R., W. F. BOTTKE, A. CARUSI, AND G. B. VALSECCHI 1991. Planetary accretion rates: Analytical derivation. *Icarus* **94,** 98–111.

GREENZWEIG, Y., AND J. J. LISSAUER 1990. Accretion rates of protoplanets. *Icarus* **87,** 40–77.

GREENZWEIG, Y., AND J. J. LISSAUER 1992. Accretion rates of protoplanets. *Icarus* **100,** 440–463.

HARRIS, A. W. 1984. The origin and evolution of planetary rings. In *Planetary Rings,* (R. Greenberg and A. Brahic, Eds.), pp. 641–659. Univ. of Arizona Press, Tucson.

HATZES, A. P., BRIDGES, F. G., AND D. N. C. LIN 1988. Collisional properties of ice spheres at low impact velocities. *Mon. Not. R. Astron. Soc.* **213,** 1091–1116.

KEMENY, J., AND J. SNELL 1960. *Finite Markov Chains.* Van Nostrand, Princeton.

LISSAUER, J. J., AND G. R. STEWART 1993. Growth of planets from planetesimals. In *Protostars and Planets III* (E. H. Levy and J. I. Lunine, Eds.), pp. 1061–1088. Univ. of Arizona Press, Tucson.

LONGARETTI, P. 1989. Saturn's main ring particle size distribution: An analytic approach. *Icarus* **81,** 51–73.

NAKAMURA, AKIKO, AND AKIRA FUJIWARA 1991. Velocity distribution of fragments formed in a simulated collisional disruption. *Icarus* **92,** 132–146.

NAKAZAWA, KIYOSHI, AND SHIGERU IDA 1988. Hill's approximation in the three-body problem. *Prog. Theor. Phys. Suppl.* **96,** 167–174.

OHTSUKI, K., Y. NAKAGAWA, AND K. NAKAZAWA 1990. Artificial acceleration in accumulation due to coarse mass-coordinate divisions in numerical simulation. *Icarus* **83,** 205–215.

OHTSUKI, K. 1992. Evolution of random velocities of planetesimals in the course of accretion. *Icarus* **98,** 20–27.

OHTSUKI, K. 1993. Capture probability of colliding planetesimals: Dynamical constraints on the accretion of plants, satellites and ring particles. *Icarus* **106,** 228–246.

PETIT, J.-M., AND M. HENON 1986. Satellite encounters. *Icarus* **66,** 536–555.

SAFRONOV, V. S. 1963. A restricted solution of the accretion equation. *Sov. Phys. Doklady* **7,** 967–969.

SALO, H. 1992. Gravitational Wakes in Saturn's Rings. *Nature* **359,** 619–621.

SALO, H. 1994. Simulations of Dense Planetary Rings. III. Self-Gravitating Identical Particles. Submitted for publication.

SHOWALTER, M. R., AND J. N. CUZZI 1993. Seeing ghosts: Photometry of Saturn's G ring. *Icarus* **103,** 124–143.

SOTER, S. 1971. The dust belts of Mars. *Cornell Center Radiophys. Space Phys. Rept.* 472.

SPAUTE, D., S. J. WEIDENSCHILLING, D. R. DAVIS, AND F. MARZARI 1991. Accretional evolution of a planetesimal swarm. I. A new simulation. *Icarus* **92,** 147–164.

STEWART, G. R., D. N. C. LIN, AND P. BODENHEIMER 1984. Collision-induced transport processes in planetary rings. In *Planetary Rings,* (R. Greenberg and A. Brahic, Eds.), pp.447–512. Univ. of Arizona Press, Tucson.

STEWART, G. R., AND G. W. WETHERILL 1988. Evolution of planetesimal velocities. *Icarus* **74,** 542–553.

TANAKA, HIDEKAZU, AND KIYOSHI NAKAZAWA 1994. Validity of the statistical coagulation equation and runaway growth of protoplanets. *Icarus* **107,** 404–412.

WEIDENSCHILLING, S. J., C. R. CHAPMAN, D. R. DAVIS, AND R. GREENBERG 1984. Ring particles: Collisional interactions and physical nature. In *Planetary Rings,* (R. Greenberg and A. Brahic, Eds.), pp. 367–415. Univ. of Arizona Press, Tucson.

WETHERILL, G. W. 1990. Comparison of analytical and physical modeling of planetesimal accumulation. *Icarus* **88,** 336–354.

WETHERILL, G. W., AND G. R. STEWART 1989. Accumulation of a swarm of small planetesimals. *Icarus* **77,** 330–357.

WETHERILL, G. W., AND G. R. STEWART 1993. Formation of planetary embryos: Effects of fragmentation, low relative velocity, and independent variation of eccentricity and inclination. *Icarus* **106,** 190–209.

ZVYAGINA, E. V., AND V. S. SAFRONOV 1972. Mass distribution of protoplanetary bodies. *Sov. Astron.* **15,** 810–817.